Article

Immunity

A Prion-like Domain in Transcription Factor EBF1 Promotes Phase Separation and Enables B Cell Programming of Progenitor Chromatin

Graphical Abstract

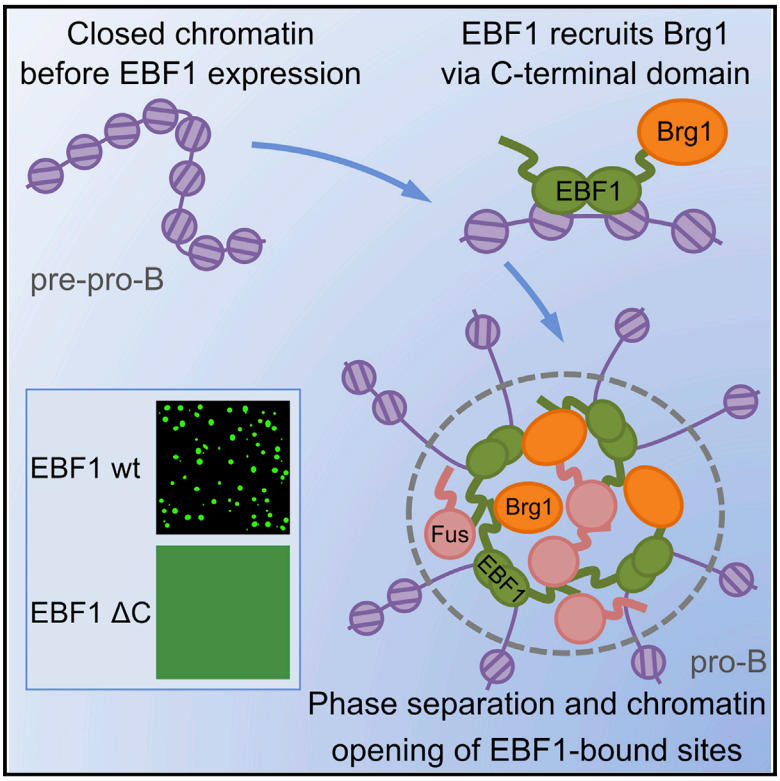

Highlights

- B lineage chromatin pioneering by EBF1 requires a prion-like domain (PLD)
- PLD stabilizes chromatin binding of EBF1 via Brg1 recruitment
- EBF1 undergoes phase separation enhanced by interaction with FUS
- Brg1 partitions into phase-separated FUS condensates

Authors

Yuanting Wang, Nikolay Zolotarev, Cheng-Yuan Yang, Angelika Rambold, Gerhard Mittler, Rudolf Grosschedl

Correspondence

grosschedl@ie-freiburg.mpg.de

In Brief

Lineage-specific programming of chromatin requires transcription factors to bind inaccessible chromatin. Wang et al. find that “pioneering” by the transcription factor EBF1 involves a prion-like domain that enables recruitment of chromatin remodelers and formation of phase-separated condensates. Partitioning of EBF1-bound sites into condensates may coordinate expression of B lineage genes.

Wang et al., 2020, Immunity *53*, 1–17
December 15, 2020
https://doi.org/10.1016/j.immuni.2020.10.009

CellPress

Immunity

CellPress

Article

A Prion-like Domain in Transcription Factor EBF1 Promotes Phase Separation and Enables B Cell Programming of Progenitor Chromatin

Yuanting Wang,[1,2] Nikolay Zolotarev,[1,2] Cheng-Yuan Yang,[1] Angelika Rambold,[1] Gerhard Mittler,[1] and Rudolf Grosschedl[1,3,*]

[1]Max Planck Institute of Immunobiology and Epigenetics, 79108 Freiburg, Germany
[2]These authors contributed equally
[3]Lead Contact
*Correspondence: grosschedl@ie-freiburg.mpg.de
https://doi.org/10.1016/j.immuni.2020.10.009

SUMMARY

Establishment of B-lineage-specific gene expression requires the binding of transcription factors to inaccessible chromatin of progenitors. The transcription factor EBF1 can bind genomic regions prior to the detection of chromatin accessibility in a manner dependent on EBF1's C-terminal domain (CTD) and independent of cooperating transcription factors. Here, we studied the mechanism whereby the CTD enables this pioneering function. The CTD of EBF1 was dispensable for initial chromatin targeting but stabilized occupancy via recruitment of the chromatin remodeler Brg1. We found that the CTD harbors a prion-like domain (PLD) with an ability of liquid-liquid phase separation, which was enhanced by interaction of EBF1 with the RNA-binding protein FUS. Brg1 also partitioned into phase-separated FUS condensates and coincided with EBF1 and FUS foci in pro-B cells. Heterologous PLDs conferred pioneering function on EBF1ΔCTD. Thus, the phase separation ability of EBF1 facilitates Brg1-mediated chromatin opening and the transition of naive progenitor chromatin to B-lineage-committed chromatin.

INTRODUCTION

Major developmental transitions including cell fate decisions require the rewiring of transcriptional regulatory networks in which changes in transcription factor ensembles lead to altered gene expression programs and different chromatin states. In particular, the generation of cell lineages in the hematopoietic system is an excellent paradigm for studying the mechanisms underlying the initiation of new gene programs. The developmental trajectory leading to cells of the B lineage consists of multipotent progenitors, lymphoid-primed progenitors, common lymphoid progenitors, and pro-B cells that progressively lose lineage potential (Boller and Grosschedl, 2014; Nutt and Kee, 2007; Rothenberg, 2014). Differentiation of these cells involves multi-lineage priming of enhancers in progenitors (Heinz et al., 2010; Laslo et al., 2006; Mercer et al., 2011), activation of new gene programs by lineage-specifying transcription factors (Lin et al., 2010), and repression of alternative lineage potential that commits cells to specific cell fates (Nechanitzky et al., 2013; Nutt and Kee, 2007; Revilla-I-Domingo et al., 2012). Multi-lineage priming in progenitors has been attributed to the functions of the transcription factors PU.1, Ikaros, and E2A (Georgopoulos, 2002; Heinz et al., 2010; Laslo et al., 2006). The inactivation of the genes encoding PU.1 or Ikaros results in developmental blocks preceding the specification of the B cell fate (Pongubala et al., 2008; Reynaud et al., 2008). The transition of common lymphoid progenitors to pro-B cells requires a cohort of transcription factors, including E2A, Foxo1, EBF1, and Pax5, that form a regulatory network underlying the generation of B lineage cells (Lin et al., 2010; Medina et al., 2004). In addition, the reshaping of progenitor chromatin during B cell programming has been found to require the Brg1/BAF chromatin remodeling complex (Bossen et al., 2015; Choi et al., 2012; Gao et al., 2009). The B-lineage-defining transcription factors cross-regulate each other's expression but seem to have distinct functions. In particular, EBF1 is at the core of this network and able to initiate B cell differentiation in *Ikaros*-deficient mice that have a developmental block at the progenitor stage (Reynaud et al., 2008; Zandi et al., 2008). Moreover, expression of EBF1 in *Ebf1*$^{-/-}$ progenitors that are arrested prior to the pro-B cell stage allows for the establishment of the B cell gene expression program and initiation of B cell differentiation, including the reshaping of progenitor chromatin (Li et al., 2018; Maier et al., 2004; Treiber et al., 2010b; Zandi et al., 2008). Thus, EBF1 has been proposed to act as a "pioneer" factor.

Pioneer transcription factors often function at developmental transitions, and they initiate new programs of gene expression. They are capable of binding inactive regulatory elements in the context of nucleosomes, promote local chromatin opening, and facilitate binding of cooperating transcription factors

Please cite this article in press as: Wang et al., A Prion-like Domain in Transcription Factor EBF1 Promotes Phase Separation and Enables B Cell Programming of Progenitor Chromatin, Immunity (2020), https://doi.org/10.1016/j.immuni.2020.10.009

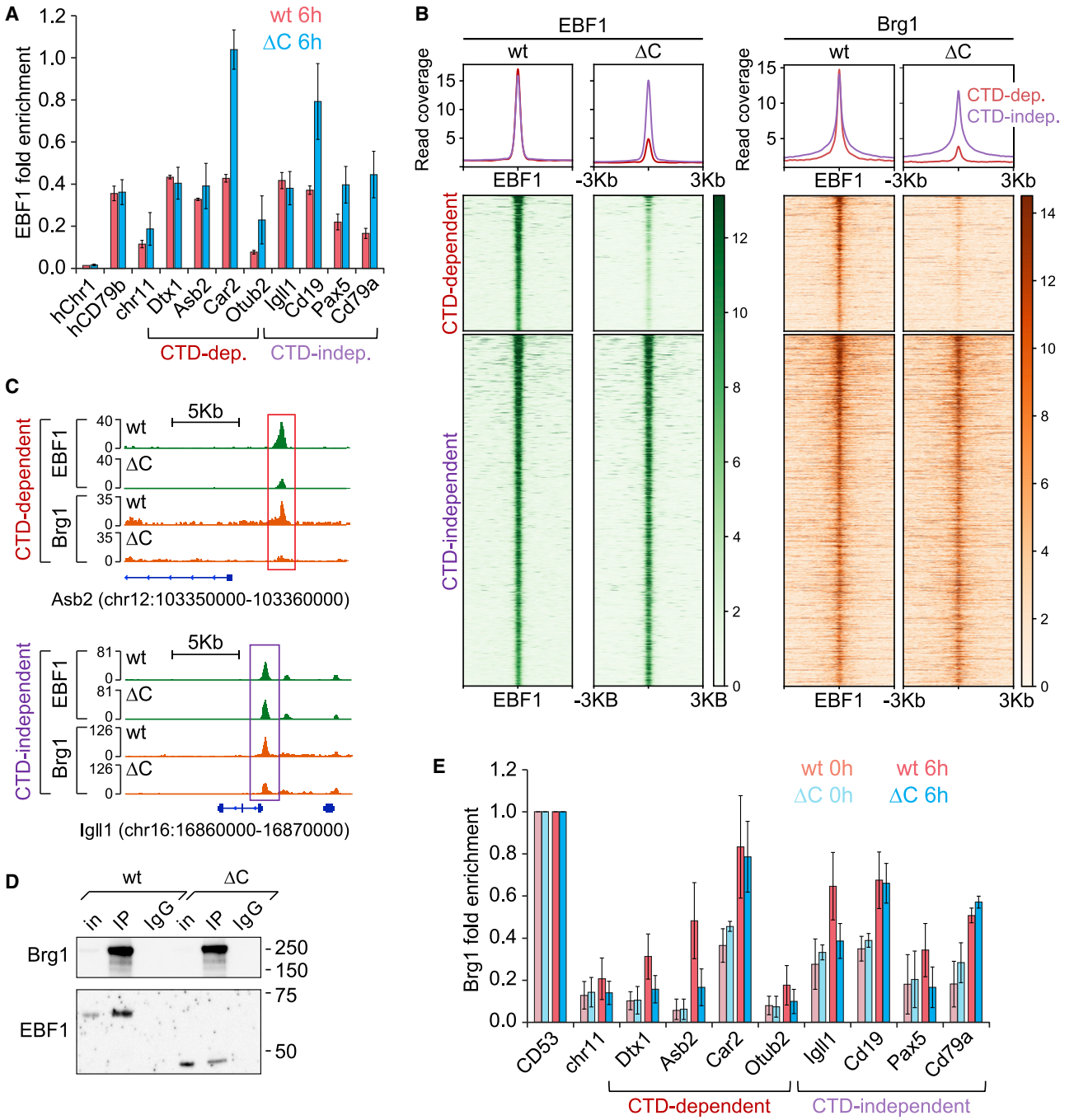

Figure 1. The CTD Is Dispensable for Initial Chromatin Targeting of EBF1 but Required for Recruitment of Brg1 to EBF1-Occupied Sites

(A) Quantitative ChIP analysis to assess binding of EBF1wt and EBF1ΔC at CTD-dependent and CTD-independent sites in *Ebf1*$^{-/-}$ "Tet-On" cells in which EBF1wt or EBF1ΔC expression was induced by doxycycline treatment for 6 h. Chromatin from human Bjab cells was spiked in for normalization. An intergenic region on chromosome 11 (chr11) served as a negative control. Error bars represent SD of three biological replicates.

(B) ChIP-seq analysis of EBF1 and Brg1 occupancy in EBF1wt- or EBF1ΔC-expressing transformed *Ebf1*$^{fl/fl}$ *RERT*^{Cre} pro-B cells in which the endogenous *Ebf1* alleles were inactivated after transduction with EBF1wt- or EBF1ΔC-expressing retroviruses. Regions ± 3 kb around EBF1 peak summits are shown. Ebf1 peaks are organized into two groups: CTD-dependent and -independent occupancy. Peaks were considered CTD dependent if the read count in the wt sample was at least 2-fold higher than that in the ΔC sample. Peaks in all samples were ordered according to EBF1wt peaks. Heatmap scale represents read coverage. The average read coverage profiles are shown above the heatmaps.

(C) Occupancy profiles of EBF1 and Brg1 in EBF1wt- or EBF1ΔC-expressing pro-B cells. Representative CTD-dependent *(Asb2)* and CTD-independent *(Igll1)* genes are shown. The vertical axis represents read coverage.

(legend continued on next page)

Please cite this article in press as: Wang et al., A Prion-like Domain in Transcription Factor EBF1 Promotes Phase Separation and Enables B Cell Programming of Progenitor Chromatin, Immunity (2020), https://doi.org/10.1016/j.immuni.2020.10.009

(Iwafuchi-Doi and Zaret, 2016; Meers et al., 2019; Zaret and Carroll, 2011). Consistent with these criteria, time-resolved analysis of inducible EBF1 expression in *Ebf1*-deficient progenitors indicated that EBF1 binds its genomic target sites within 6 h of induction, preceding the formation of chromatin accessibility and transcriptional activation of genes that occur between 24 and 72 h of induction (Li et al., 2018).

EBF1 is a multi-domain transcription factor consisting of a large DNA-binding domain (DBD) followed by an IPT (Ig-like/plexins/transcription factors) domain, helix-loop-helix (HLH) dimerization domain, and large C-terminal domain (CTD; Hagman, 1983). The CTD is important for the activation of a specific set of EBF1 target genes, termed CTD-dependent genes, which are involved in the early B cell fate decision (Boller et al., 2016). In contrast, a larger set of EBF1 target genes, termed CTD-independent genes, is equally regulated by both wild-type EBF1 and EBF1 lacking the CTD (EBF1ΔC). Notably, the CTD has no typical transactivation activity, but it facilitates EBF1 chromatin binding and DNA demethylation at regulatory regions that have very few binding sites for collaborating transcription factors (Boller et al., 2016; Hagman et al., 1995). The CTD lacks predicted secondary structure and had to be removed for crystallization of EBF1, suggesting that it represents an intrinsically disordered region (IDR) (Treiber et al., 2010a). However, the mechanism by which the CTD confers pioneering activity is still obscure.

Intrinsically disordered protein regions are characterized by a low sequence complexity and often resemble prion-like domains (PLDs). In particular, PLDs can form reversible biomolecular condensates in a process of liquid-liquid demixing, termed phase separation, in which specific proteins partition into condensates whereas others are kept out (Kato et al., 2012; Malinovska et al., 2013). Liquid-liquid phase-separated condensates represent membrane-less compartments, such as the nucleolus, stress granules, and nuclear or cytoplasmic speckles, which concentrate various biochemical processes within cells (Banani et al., 2017; Hyman et al., 2014). Phase separation has been extensively studied for RNA-binding proteins of the FET family of proteins, which includes FUS, EWSR1, and TAF15 (Schwartz et al., 2015; Wang et al., 2018). These proteins have PLDs containing polar and aromatic residues that drive phase separation as autonomous units and in collaboration with other IDRs enriched in positively charged amino acids (Wang et al., 2018). In addition, many transcription factors contain activation domains that form phase-separated condensates in combination with the Mediator coactivator MED1 and the acetyl-lysine reader BRD4 at super-enhancers (Sabari et al., 2018). Moreover, signaling-dependent and cooperative enhancer assembly has been linked to phase separation by transcription factors and enhancer RNA (Nair et al., 2019).

Here, we analyzed the mechanism by which the CTD contributes to shaping the chromatin landscape during EBF1-mediated B cell programming. We found that the function of the CTD depends on a PLD with phase separation ability, which was further enhanced by an interaction with FUS. The PLD was not required for initial chromatin binding, but it allowed for the recruitment of Brg1. We propose that phase separation by EBF1 in combination with FET family proteins facilitates Brg1-mediated chromatin opening and coordination of gene expression in B lymphopoiesis.

RESULTS

The CTD Is Dispensable for Initial Chromatin Targeting of EBF1 but Required for Brg1 Recruitment

The CTD of EBF1 confers "pioneering" of naive progenitor chromatin and enables the activation of a specific set of genes, termed CTD-dependent genes, that are involved in the B cell fate decision (Boller et al., 2016). These genes contain regulatory regions in which chromatin binding by EBF1 occurs in the absence of cooperating transcription factors. In contrast, the set of CTD-independent genes is characterized by EBF1 binding in association with other transcription factors (Boller et al., 2016). Although the pioneering function of CTD has been established, the underlying mechanism is still obscure. In a previous study, we showed that EBF1 binds chromatin prior to the formation of chromatin accessibility (Li et al., 2018). To address the question of whether the CTD is required for initial chromatin binding, we used the same approach and generated *Ebf1*$^{-/-}$ Tet-On progenitor cells harboring doxycyclin-inducible EBF1wt- or EBF1ΔC-expressing gene constructs (Figures S1A and S1B). Quantitative EBF1 ChIP analysis indicated that EBF1ΔC binding occurred at both CTD-dependent and -independent sites with equal or even higher efficiency than EBF1wt binding at 6 h of induction (Figures 1A). In this experiment, we spiked in chromatin from human Bjab B cells to enable a quantitative comparison of EBF1 occupancy in EBF1wt- and EBF1ΔC-expressing cells. Together with our previous findings, these results show that EBF1ΔC can initially bind naive chromatin of CTD-dependent targets with similar efficiency as EBF1wt but lacks the ability of stable binding, which requires the CTD and the possible recruitment of cofactors.

To identify possible cofactors that are important for the activity of the CTD domain, we initially took a candidate approach. Brg1 (Smarca 4), the catalytic subunit of the BAF chromatin remodeling complex, has been associated with the pioneering activity of transcription factors, such as GATA3 and Oct4 (King and Klose, 2017; Takaku et al., 2016). Moreover, Brg1 is involved in establishing a *de novo* enhancer repertoire in lymphoid progenitors and is required for the efficient generation of pro-B cells (Bossen et al., 2015). Therefore, we examined whether the chromatin binding by EBF1 involves the recruitment of Brg1. An analysis of publicly available ChIP-seq (chromatin immunoprecipitation sequencing) data of EBF1 and Brg1 occupancy in pro-B cells suggested that EBF1 peaks overlap with weak Brg1 peaks (Figure S1C). To examine how CTD-dependent and -independent

(D) Co-immunoprecipitation of Brg1 and EBF1wt or EBF1ΔC proteins from lysates of pro-B cells. Proteins were immunoprecipitated with anti-Brg1 antibody, and the immunoblots were probed with anti-Brg1 or anti-FLAG-HRP antibodies. In represents 0.5% input. IgG was used as a control. Immunoblot is representative of four experiments.

(E) Quantitative ChIP analysis to detect binding of Brg1 to EBF1 CTD-dependent and CTD-independent sites in *Ebf1*$^{-/-}$ "Tet-On" cells in which EBF1wt or EBF1ΔC expression was induced by doxycycline treatment for 6 h. Brg1 binding was normalized to an EBF1-independent Brg1 site in the *Cd53* locus. Error bars represent SD of two biological replicates.

Please cite this article in press as: Wang et al., A Prion-like Domain in Transcription Factor EBF1 Promotes Phase Separation and Enables B Cell Programming of Progenitor Chromatin, Immunity (2020), https://doi.org/10.1016/j.immuni.2020.10.009

EBF1 occupancy relate to the recruitment of Brg1, we analyzed Brg1 binding at CTD-dependent and -independent sites in EBF1wt and EBF1ΔC-expressing pro-B cells. Toward this end, we adopted a gene replacement strategy in *Ebf1*$^{fl/fl}$*RERT*^{Cre} pro-B cells in which we inactivated the endogenous floxed *Ebf1* alleles after the transduction with EBF1wt or EBF1ΔC-expressing retroviruses (Boller et al., 2016). For the ChIP-seq analysis, we used a newly available α-Brg1 antibody that allowed for the detection of more and stronger Brg1 peaks relative to the study by Bossen et al., whereby 90% of the previously detected Brg1 peaks were included in the new dataset (Figure S1D). By clustering Brg1 peaks according to an overlap with CTD-dependent and -independent EBF1 peaks, we found that the recruitment of Brg1 correlates with EBF1 occupancy (Figure 1B). In particular, we observed reduced Brg1 binding at CTD-dependent sites of EBF1 occupancy in EBF1ΔC-expressing cells relative to EBF1wt-expressing cells but similar Brg1 binding at CTD-independent sites. This difference of Brg1 recruitment to CTD-dependent EBF1-occupied sites in EBF1wt- versus EBF1ΔC-epressing cells was also seen for specific genes (Figures 1C and S1E). We also examined the interaction of Brg1 and EBF1 in lysates of EBF1wt- and EBF1ΔC-expressing pro-B cells by co-immunoprecipitation. In this experiment, we found a diminished interaction of Brg1 with EBF1ΔC relative to EBF1wt (Figure 1D). Thus, the recruitment of Brg1 to EBF1-occupied sites involves an interaction with the CTD.

We also examined the recruitment of Brg1 to sites of EBF1 occupancy at 6 h after doxycylin induction of EBF1 expression, when the binding of EBF1wt and EBF1ΔC to naive chromatin was similar. In EBF1wt-expressing cells, Brg1 is recruited to both CTD-dependent and -independent sites (Figure 1E). In EBF1ΔC-expressing cells, however, we did not detect significant Brg1 binding except at sites associated with the *Car2*, *Cd19*, and *Cd79a* genes. Therefore, we considered the possibility that the recruitment of Brg1 to these sites is governed by another transcription factor(s). In particular, PU.1, which is expressed in *Ebf1*$^{-/-}$ progenitor cells prior to the induction of EBF1 expression (Li et al., 2018), has been assigned pioneer function and can recruit Brg1 (Heinz et al., 2010; Minderjahn et al., 2020; Ungerbäck et al., 2018). ChIP analysis of PU.1 binding in uninduced *Ebf1*$^{-/-}$ Tet-On cells and interrogation of previously published ChIP-seq data in pro-B cells indicated that the sites associated with *Car2*, *Cd19*, and *Cd79a*, but not the other analyzed sites, are occupied by PU.1 (Figures S1F and S1G). Therefore, the CTD-independent Brg1 recruitment could be supported by another transcription factor such as PU.1, suggesting that the recruitment of Brg1 to sites of EBF1 occupancy is governed by the CTD of EBF1 or by colocalized transcription factors such as PU.1.

A Short Region of the CTD Is Necessary and Sufficient for the Pioneering Function of EBF1

To gain further insight into the mechanism underlying the function of the large CTD, we delineated the functionally important region for transcriptional activation of CTD-dependent genes. To this end, we generated C-terminal truncations of EBF1 (Figure S2A). After transduction of developmentally arrested *Ebf1*$^{-/-}$ progenitor cells with retroviruses expressing wild-type or C-terminally truncated EBF1 proteins along with GFP, we sorted GFP$^+$CD19$^+$ cells and confirmed the similar expression of full-length and truncated EBF1 proteins by immunoblot analysis (Figure S2B). In the sorted cells, we also assessed the expression of CTD-dependent and CTD-independent target genes of EBF1 by qRT-PCR analysis. C-terminal truncations up to amino acid 520 had no detectable effects on the activation of the EBF1 target genes examined (Figure S2C). Further truncations to amino acid 500 had a partial effect specifically on CTD-dependent target genes, whereas the removal of an additional 20 amino acids reduced their expression to a similar low level as observed with EBF1ΔC-transduced cells. Importantly, none of these truncations had an effect on the activation of the CTD-independent targets. We further examined the effects of an internal deletion of amino acids 480–520 and found that this mutant, termed Δ480-520, resembled EBF1ΔC in its reduced ability to activate CTD-dependent genes (Figures 2A–2C). Conversely, the fusion of amino acids 480–520 onto the C terminus of EBF1ΔC, termed F480-520, allowed for the activation of CTD-dependent genes at levels similar to those observed with EBF1wt. Thus, a relatively small region of the CTD is necessary and sufficient for the activation of CTD-dependent target genes.

We have previously shown that the removal of the CTD also affects the ability of EBF1 to regulate the differentiation of progenitor cells to CD19$^+$ pro-B cells (Boller et al., 2016). Therefore, we used flow cytometry to analyze the differentiation of GFP$^+$ progenitor cells transduced with wild-type or mutant EBF1-expressing retroviruses. We used the cell surface markers CD19 and BP1 to distinguish CD19$^+$BP1$^-$ early pro-B and CD19$^+$BP1$^+$ late pro-B cells. EBF1wt-transduced progenitors yielded ~99% CD19$^+$ cells with the vast majority identified as late pro-B cells (Figures 2D and 2E). In contrast, EBF1ΔC-transduced progenitors generated slightly fewer CD19$^+$ cells that included earlier than late pro-B cells. Similar ratios of early versus late pro-B cells were observed with Δ480-520-expressing progenitors. In contrast, F480-520-transduced cells generated late pro-B cells at similar frequencies to EBF1wt-transduced progenitors (Figures 2D and 2E). Taken together, these experiments indicate that the amino acids 480−520 confer upon EBF1 the ability to activate a specific set of genes in progenitors and to promote the efficient developmental progression of these cells.

The Functionally Defined Region of the CTD Interacts with Proteins of the FET Family

To identify interaction partners of the functionally delineated CTD region, we employed stable isotope labeling with amino acids in cell culture (SILAC) and mass spectrometry with lysates of 38B9 pro-B cells. Previous SILAC experiments, in which we analyzed lysates of EBF1wt- and EBF1ΔC-expressing pro-B cells did not yield differentially enriched proteins (Boller et al., 2016; unpublished data). As the interactions of the CTD with proteins may be weak, we used synthetic labeled peptides, encompassing amino acids 460−520 or 532−591 of EBF1 (Figure S3A). In six independent experiments, including forward and reverse SILAC labeling, we identified 128 proteins that were reproducibly enriched with the 460−520 peptide by more than 4-fold relative to the 532−591 peptide. Notably, we consistently identified three members of the FET family: FUS, EWSR1, and TAF15, which were enriched by the 460−520 peptide with similar

Please cite this article in press as: Wang et al., A Prion-like Domain in Transcription Factor EBF1 Promotes Phase Separation and Enables B Cell Programming of Progenitor Chromatin, Immunity (2020), https://doi.org/10.1016/j.immuni.2020.10.009

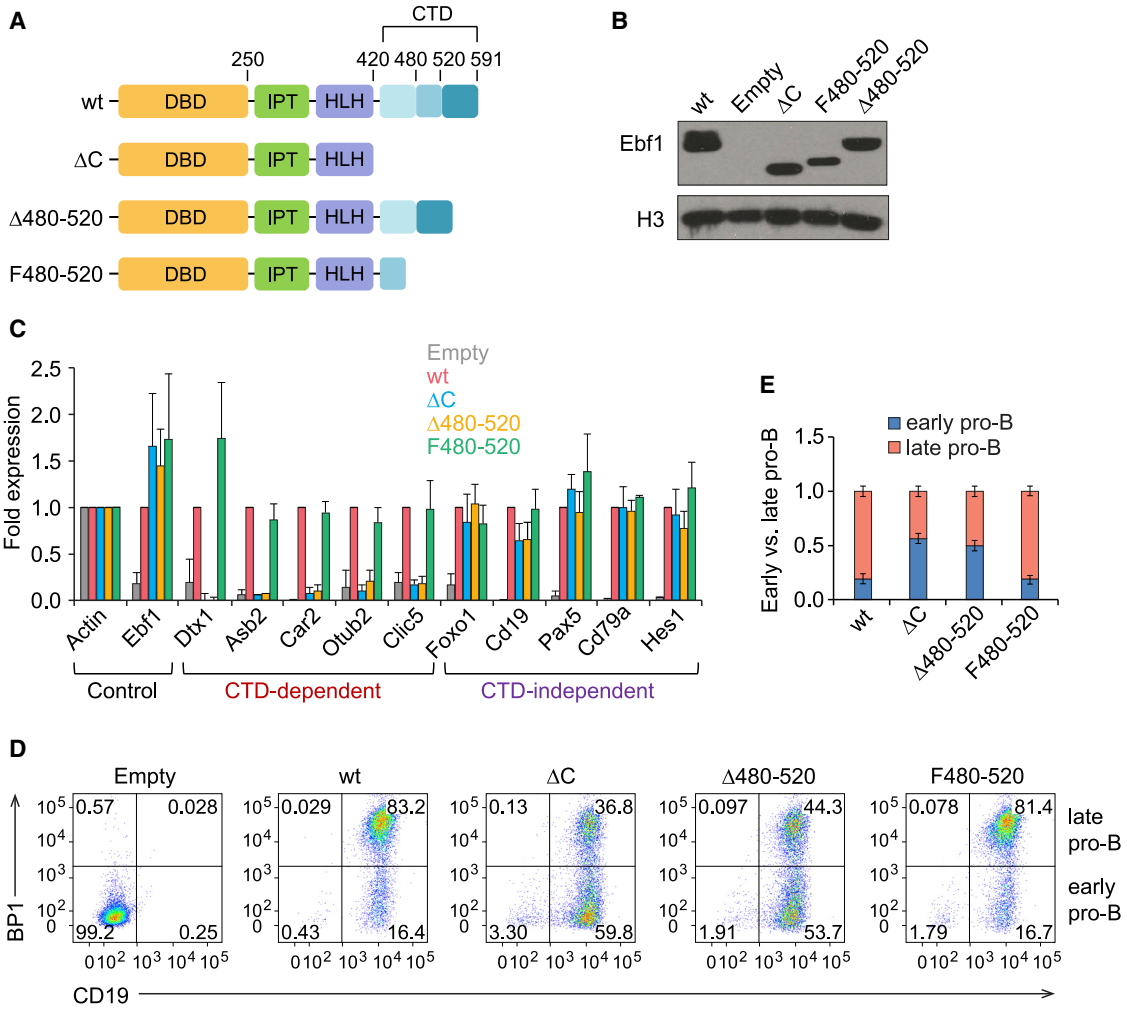

Figure 2. A Short Region Is Necessary and Sufficient for EBF1 C Terminus Function

(A) Domain structures of EBF1wt, EBF1ΔC, EBF1 lacking amino acids 480–520 (Δ480-520), and EBF1 in which the C terminus is replaced with amino acids 480–520 (F480-520). The DNA binding domain (DBD), IPT domain, helix-loop-helix domain (HLH), and the C-terminal domain (CTD) with the positions of amino acids indicated are shown.

(B) Immunoblot analysis to assess the expression of EBF1 proteins in *Ebf1*$^{-/-}$ cells transduced with various EBF1-GFP bicistronic retroviruses as indicated. H3 is a loading control.

(C) qRT-PCR analysis to assess transcription of control genes, CTD-dependent genes and CTD-independent genes in cells expressing empty vector, EBF1wt, or various EBF1 mutants. Raw cycle values were first normalized to actin and are represented as fold expression relative to EBF1wt-expressing cells. Error bars represent SD of three biological replicates.

(D) Representative flow cytometric analysis to detect BP1 and CD19 expression on GFP-positive cells that have been transduced with EBF1wt, EBF1ΔC, Δ480, or F480-520 2 weeks prior to analysis. Percentages of CD19^{+}BP1^{-} early pro-B and CD19^{+}BP1^{+} late pro-B cells are indicated.

(E) Ratio of early pro-B versus late pro-B cells. Error bars represent SD from three biological replicates.

efficiency and significance (Figure 3A). We confirmed these interactions by pull-down experiments, using the 460–520 and 532–591 EBF1 peptides and lysates from HEK293T cells that were transfected with epitope-tagged expression plasmids for FUS, EWSR1, and TAF15 (Figure 3B).

FET proteins are RNA-binding proteins that comprise domains of low sequence complexity, also referred to as PLDs (Harrison and Shorter, 2017). These proteins form reversible liquid-liquid phase-separated droplets whereby the interaction between related PLDs and RNA-binding domains drive the formation of condensates at near physiological concentrations (Wang et al., 2018). To examine whether the apparently unstructured CTD of EBF1 (Treiber et al., 2010a) confers similar properties, we first analyzed the primary sequence of EBF1 with the PLAAC algorithm, which evaluates the amino acid compositional similarity with yeast prion domains (Lancaster et al., 2014). This analysis identified a region in the CTD between amino acids 460–520 that is enriched in hydrophobic and polar uncharged amino acids and may comprise a PLD (Figures 3C and S3B). Thus, the CTD includes a region that interacts with FET proteins and shows similarity to PLDs with phase separation ability.

Please cite this article in press as: Wang et al., A Prion-like Domain in Transcription Factor EBF1 Promotes Phase Separation and Enables B Cell Programming of Progenitor Chromatin, Immunity (2020), https://doi.org/10.1016/j.immuni.2020.10.009

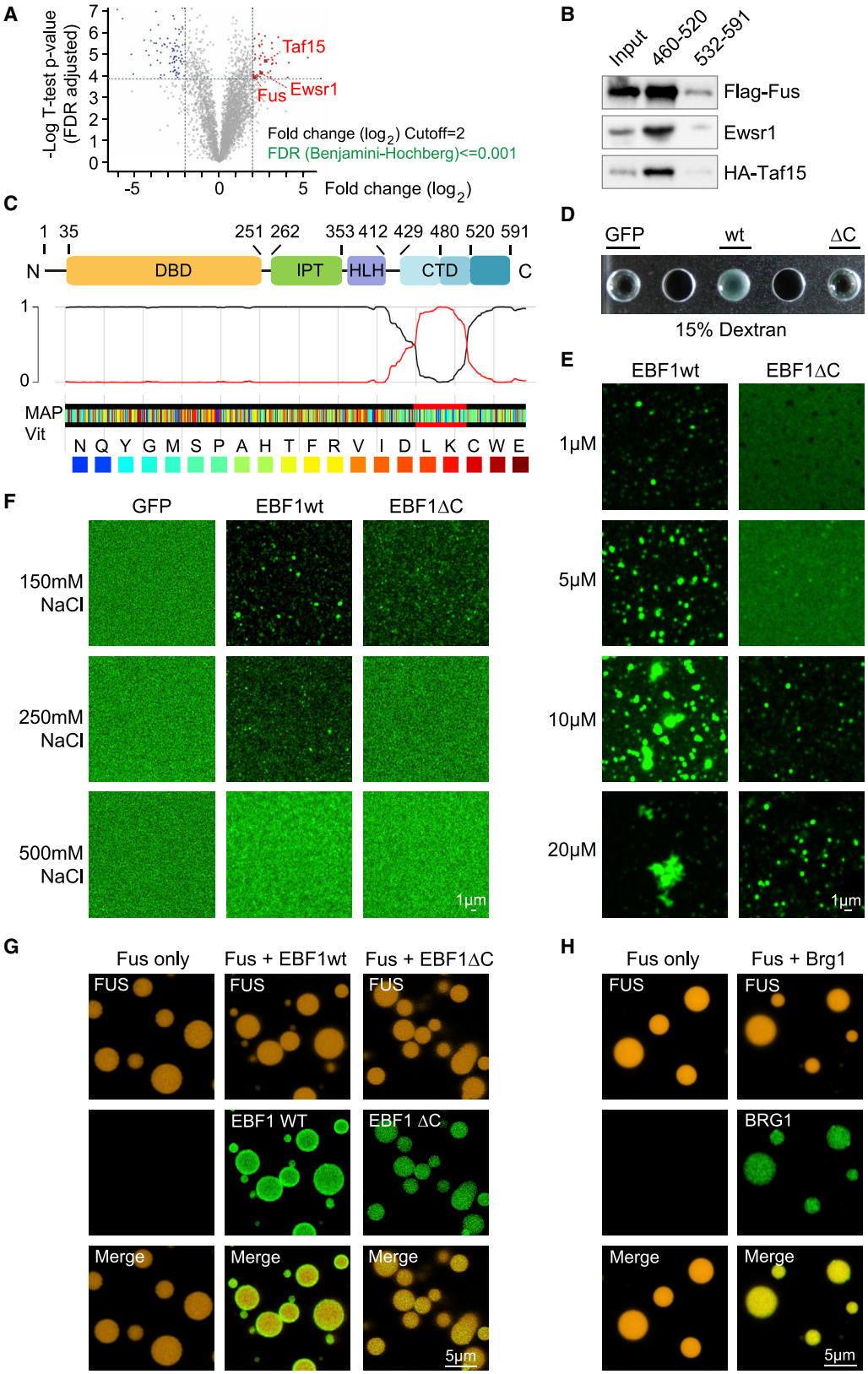

(legend on next page)

Please cite this article in press as: Wang et al., A Prion-like Domain in Transcription Factor EBF1 Promotes Phase Separation and Enables B Cell Programming of Progenitor Chromatin, Immunity (2020), https://doi.org/10.1016/j.immuni.2020.10.009

The CTD Confers upon EBF1 the Ability of Phase Separation *In Vitro*

To examine the potential phase separation capacity of EBF1wt *in vitro* and to compare it with that of EBF1ΔC, we expressed and purified recombinant MBP-GFP-EBF1 fusion proteins from insect cells and measured the turbidity of the solution in which we added dextran as a molecular crowding agent (Figures 3D, 3E, and S3C). At the protein concentration of 18 μM, the solution containing EBF1wt was turbid, whereas the solutions with EBF1ΔC and GFP were relatively clear (Figure 3D). Analysis of protein condensation by fluorescence microscopy indicated that the solution with EBF1wt formed amorphous and fibrillar condensates, whereas EBF1ΔC formed fewer and smaller condensates (Figure S3D). The formation of phase-separated condensates is influenced by protein and salt concentrations (Alberti et al., 2019; Hyman et al., 2014). Therefore, we examined condensate formation at varying protein concentrations and found that EBF1wt formed spherically shaped condensates at 1 μM, whereas no obvious condensates were detected with EBF1ΔC at this protein concentration (Figure 3E). At 10 μM protein concentration, EBF1wt formed already amorphous and fibrillary structures, whereas EBFΔC formed condensates that resembled those of EBF1wt condensates formed at 1 μM. Quantification of the phase separation properties of EBF1wt and EBF1ΔC confirmed the ability of the CTD to enhance the phase behavior of EBF1 (Figure S3E). We also examined the formation of the EBF1 condensates at different salt concentrations and without dextran (Figure 3F). At 500 mM salt concentration, both EBF1wt and EBF1ΔC were fully soluble. At 250 mM salt, only EBF1wt formed small condensates and at 150 mM salt, EBF1ΔC and EBF1wt formed small and larger condensates, respectively (Figure 3F). Importantly, the EBF1ΔC and EBF1wt condensates could, at least in part, be reversibly solubilized by increasing the salt concentration, suggesting that the condensates are not aggregates that are irreversible (Figure S3F). Thus, the CTD confers upon EBF1 the capacity of forming condensates that respond to changes in salt concentration with adjustments in size, a feature characteristic of phase-separated condensates formed by multiple weak protein-protein interactions (Alberti et al., 2019).

FUS and EWSR1 form condensates *in vitro* that are larger than those observed with EBF1 (Qamar et al., 2018; Wang et al., 2018). Based on the interaction of the EBF1 460–520 peptide with FUS and EWSR1, we examined whether or not the phase separation ability of EBF1 is enhanced in the presence of FUS. To this end, we mixed SNAP-tagged FUS at 10 μM with EBF1wt-GFP or EBF1ΔC-GFP at 1 μM and assessed the formation of condensates by fluorescence microscopy. By itself, FUS protein formed condensates with an average diameter of ~5 μm (Figure 3G). Incubation of EBF1wt-GFP together with FUS formed condensates with both proteins, suggesting that EBF1 partitions efficiently into FUS condensates (Figure 3G). In contrast, EBF1ΔC was less efficiently included into FUS condensates (Figures 3G and S3G). Thus, the CTD mediates not only condensate formation by EBF1 but also enhances its inclusion into FUS condensates. However, the deletion of the CTD was not sufficient to abrogate partitioning of EBF1 into FUS condensates. Efficient phase transition of FUS involves interactions of the N-terminal PLD with a C-terminal arginine-rich domain (Qamar et al., 2018; Wang et al., 2018) and therefore, FUS may interact with EBF1ΔC via an additional domain of EBF1.

FET proteins have been found to interact with Brg1 and recruit Brg1 to chromatin in oncogenic fusion with the DNA-binding domains of Fli1 or DDIT3 (Boulay et al., 2017; Lindén et al., 2019). Therefore, we also assessed the ability of purified Brg1 for the recruitment into FUS condensates *in vitro* by incubating purified and labeled Brg1 with FUS. We observed that Brg1 is efficiently included into FUS droplets (Figure 3H). Thus, EBF1 may target Brg1 via a common interaction with proteins of the FET family.

EBF1wt Forms 1,6 Hexanediol-Sensitive and Dynamic Foci and Colocalizes with FUS and Brg1

To extend these observations and examine the phase separation ability of EBF1wt versus EBF1ΔC *in vivo*, we transduced *Ebf1*$^{-/-}$ progenitor cells with retroviruses expressing mCherry-EBF1 fusion proteins at levels comparable to that detected in sorted primary pro-B cells (Figure S4A). Confocal microscopy indicated

Figure 3. Amino Acids 480–520 Form a Prion-like Domain that Enables Phase Separation of EBF1 *In Vitro*

(A) Volcano blot of the mass spectrometry analysis of proteins that were enriched from nuclear extracts of SILAC-labeled pro-B cells with the EBF1(460-520) peptide relative to the EBF1(532-591) peptide. The data are the average of three biological replicates. The members of the FET family (FUS, EWSR1, and TAF15) are indicated.

(B) Interaction of FET proteins with EBF1(460-520) by peptide pull-down. Cell lysates of HEK293T cells, transfected with expression constructs of Flag-FUS, EWSR1, or HA-Taf15, were used for pull-down with EBF1(460-520) and EBF1(532-591) peptides. Antibodies directed against Flag, EWSR1, and HA were used to detect the interaction.

(C) Schematic diagram of EBF1 domains and prediction of intrinsic disorder tendency by the PLAAC algorithm (http://plaac.wi.mit.edu). A scheme of the primary sequence of EBF1, with individual amino acids color coded, is shown below (abbreviation of EBF1 domains is the same as in legend to Figure 2A).

(D) Turbidity analysis to visualize phase separation of MBP-GFP (GFP), MBP-GFP-EBF1wt (EBF1wt), and MBP-GFP-EBF1ΔC (EBF1ΔC) at 18 μM each. 15% dextran was added as a crowding agent.

(E) Fluorescence microscopy images of protein condensates by MBP-GFP-EBF1wt and MBP-GFP-EBF1ΔC at increasing protein concentrations (1–20 μM) in 15% dextran. Scale bar is 1 μm.

(F) Fluorescence microscopy images of phase-separated droplet formation by MBP-GFP, MBP-GFP-EBF1wt, or MBP-GFP-EBF1ΔC (6 μM each) at the indicated NaCl concentrations. Scale bar is 1 μm.

(G) Fluorescence microscopy images of droplet formation by 10 μM purified Alexa 546-labled SNAP-tagged FUS protein alone or in combination with 1 μM MBP-GFP-EBF1wt or MBP-GFP-EBF1ΔC in buffer with 150mM NaCl and 5% dextran. Images were taken 10 min after incubation at room temperature. Scale bar is 5 μm.

(H) Analysis of phase-separated droplet formation by fluorescence microscopy to detect condensate formation by Brg1 and FUS. 10 μM SNAP-Surface Alexa Fluor 546-labeled FUS was incubated alone (left panels) or in combination with 0.05 μM RED-tris-NTA-647-labeled His-Brg1 (right panels) in 150 mM NaCl and 5% dextran. Brg1 is pseudo-colored with green and FUS with orange. Scale bar, 5 μm.

Please cite this article in press as: Wang et al., A Prion-like Domain in Transcription Factor EBF1 Promotes Phase Separation and Enables B Cell Programming of Progenitor Chromatin, Immunity (2020), https://doi.org/10.1016/j.immuni.2020.10.009

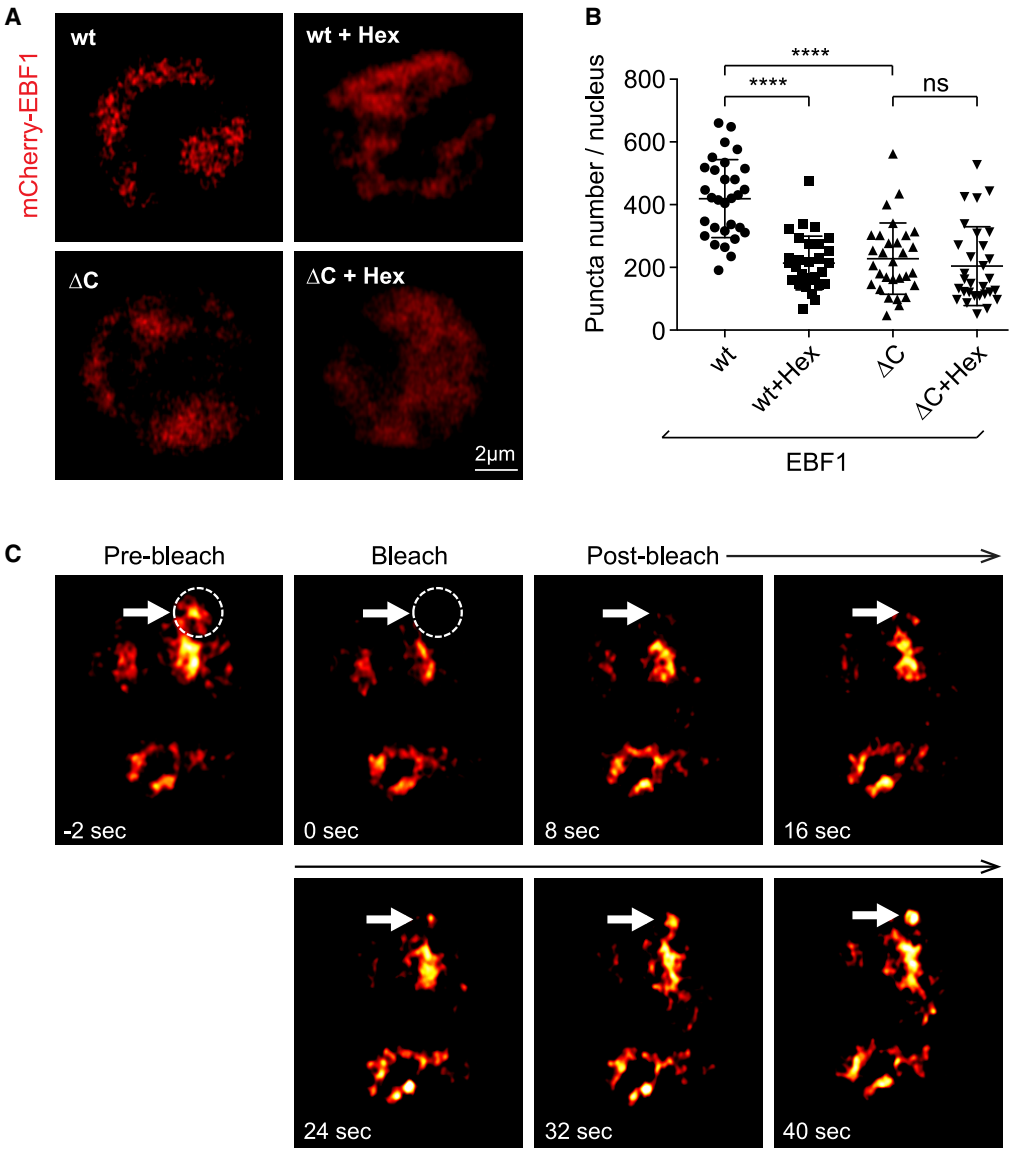

(legend on next page)

Please cite this article in press as: Wang et al., A Prion-like Domain in Transcription Factor EBF1 Promotes Phase Separation and Enables B Cell Programming of Progenitor Chromatin, Immunity (2020), https://doi.org/10.1016/j.immuni.2020.10.009

that mCherry-EBF1wt forms more and larger nuclear foci than mCherry-EBF1ΔC (Figure 4A). Liquid phase-separated condensates can be disassembled by the addition of the aliphatic alcohol 1,6-hexanediol, which perturbs weak hydrophobic interactions (Molliex et al., 2015; Strom et al., 2017). Notably, the addition of 1,6-hexanediol reduced the numbers of EBF1wt foci to a level observed with EBF1ΔC, which did not significantly change upon 1,6-hexanediol addition (Figures 4A and 4B). We obtained similar results with altered diameter thresholds for puncta detection and confirmed the reduction of the number of endogenous EBF1 foci by 1,6-hexanediol in 38B9 pro-B cells (Figures S4B–S4D).

Another key feature of liquid-like biomolecular condensates is their dynamic reorganization and exchange kinetics (Carrero et al., 2003). To probe the dynamic properties of the EBF1 puncta, we determined the kinetics of fluorescence recovery after photobleaching (FRAP) in mCherry-EBF1wt-expressing primary cells. After photobleaching, mCherry-EBF1wt puncta recovered within 40 s (Figures 4C and S4E). This kinetics is similar to those of other reported liquid-like condensates (Lin et al., 2015; Nair et al., 2019). We also performed FRAP experiments at lower image but higher kinetic resolution to quantify the dynamic properties of mCherry-EBF1wt and mCherry-EBF1ΔC in relation to mCherry (Figure 4D). mCherry-EBF1wt recovered to ~50% within 5 s and leveled off at 75% within 20 s. In contrast, mCherry-EBF1ΔC recovered with similar initial kinetics but reached almost 100% within 20 s (Figure 4D). The similar kinetics for mCherry-EBF1wt and mCherry-EBF1ΔC may be accounted for by an interaction with other proteins capable of phase separation, such as FUS. Full FRAP recovery was also observed with mCherry, although its kinetics was much faster than those of EBF1 proteins as expected for a soluble protein. Taken together, these experiments suggest that EBF1 can undergo phase separation via the PLD of the CTD *in vivo*.

EBF1 interacts with both Brg1 and FUS via the CTD *in vitro*, and we therefore examined whether the EBF1 foci detected *in vivo* colocalize with FUS and/or Brg1. To this end, we analyzed mCherry-EBF1wt- and mCherry-EBF1ΔC-expressing primary cells by confocal microscopy (Figures S5A and S5B). This analysis indicated that EBF1wt foci colocalize with both Brg1 and FUS *in vivo*. Moreover, we used the Imaris software to quantify the degree of colocalization between the fluorophores by determining the Pearson's correlation coefficient. We found a relatively high degree of colocalization between EBF1wt and Brg1, as well as between EBF1wt and FUS (Figures S5C and S5D). The colocalization was modestly but significantly reduced for EBF1ΔC and Brg1 but was not significantly changed for EBF1ΔC and FUS (Figures S5C and S5D). We also detected colocalization of endogenous EBF1 with Brg1 and FUS in 38B9 pro-B cells (Figures S5E and S5F).

The CTD Can Be Functionally Replaced by Heterologous PLDs with Phase Separation Ability

To further examine whether the function of the CTD involves its phase separation ability rather than a specific amino acid sequence, we replaced the CTD of EBF1 with heterologous domains that enable phase separation. Toward this end, we generated bicistronic GFP retroviral constructs in which EBF1ΔC is fused with the N-terminal IDR of FUS (F-Fus) or EWSR1 (F-Ewsr1) that have been well characterized as PLDs (Figure 5A). Immunoblot analysis of the transduced *Ebf1*$^{-/-}$ progenitor cells indicated that that EBF1wt and EBF1ΔC are expressed more abundantly than the F-Fus and F-Ewsr1 fusion proteins (Figure 5B). However, quantitative RT-PCR analysis aimed at detecting EBF1-mediated expression of CTD-dependent and -independent genes in GFP^{+} cells indicated that the fusion proteins activated both sets of EBF1 target genes even more efficiently than EBF1wt (Figure 5C).

The transcription factor GATA3 contains a large IDR with phase separation ability that includes two domains, termed TA1 and TA2 (Nair et al., 2019; Ranganath and Murphy, 2001; Takaku et al., 2016). In particular, the N-terminal TA1 domain enhances chromatin binding of GATA3 and mediates the recruitment of Brg1 (Takaku et al., 2016). To examine whether the TA1 of GATA3 could functionally replace the CTD of EBF1, we generated a retroviral fusion construct, termed F-GATA3, in which the TA1 domain was linked to the EBF1ΔC (Figure 5A). Transduction of *Ebf1*$^{-/-}$ progenitor cells with F-GATA3 indicated a full rescue of the expression of CTD-dependent genes relative to EBF1ΔC-transduced cells (Figure 5D). Moreover, the expression of F-GATA3 allowed for a partial rescue of the differentiation potential of the progenitor cells (Figures 5E and 5F). Thus, the CTD of EBF1 could be functionally replaced by heterologous protein domains that share the ability of phase separation, suggesting that the physical properties and not the specific amino acid sequence are important for CTD function.

The PLD of EBF1 Stabilizes Brg1 Occupancy at CTD-Dependent Genes

To assess the role of the short PLD for the interaction of EBF1 with Brg1, we performed co-immunoprecipitations with lysates of progenitor cells, transduced with retroviruses encoding EBF1wt, Ebf1ΔC, and Δ480-520. We also tested the interaction of Brg1 with the F-GATA3 fusion protein carrying a heterologous PLD. In these experiments, we detected strong solution interactions of Brg1 with EBF1wt and F-GATA3 but reduced interactions with EBF1ΔC and Δ480-520 (Figure 6A). The interaction

Figure 4. EBF1 Forms Liquid-like and Dynamic Puncta *In Vivo*

(A) *Ebf1*$^{-/-}$ pre-pro-B progenitor cells expressing mCherry EBF1 were treated with 5% 1,6-Hexanidol (Hex) for 30 s or untreated and analyzed by confocal microscopy. Representative z stack images are shown. Scale bar, 2 μm.

(B) Analysis of the numbers of puncta in the entire nuclear volume of individual cell nuclei (n = 30) by confocal microscopy and automatic calculation with the Imaris software. Each dot, square, or triangle represents a single cell. ****$p < 0.0001$; ns, non-significant.

(C) Fluorescence recovery after photo-bleaching (FRAP) analysis to analyze the dynamics of mCherry-EBF1 puncta in a pro-B cell. Images were taken at indicated time points (seconds) after photobleaching.

(D) Fluorescence recovery of EBF1 puncta in mCherry-EBF1-expressing pro-B cells (n = 10). Each dot represents the mean intensity of normalized fluorescence at the indicated time points of photo-bleaching (seconds). Error bars represent SD from 10 samples.

Please cite this article in press as: Wang et al., A Prion-like Domain in Transcription Factor EBF1 Promotes Phase Separation and Enables B Cell Programming of Progenitor Chromatin, Immunity (2020), https://doi.org/10.1016/j.immuni.2020.10.009

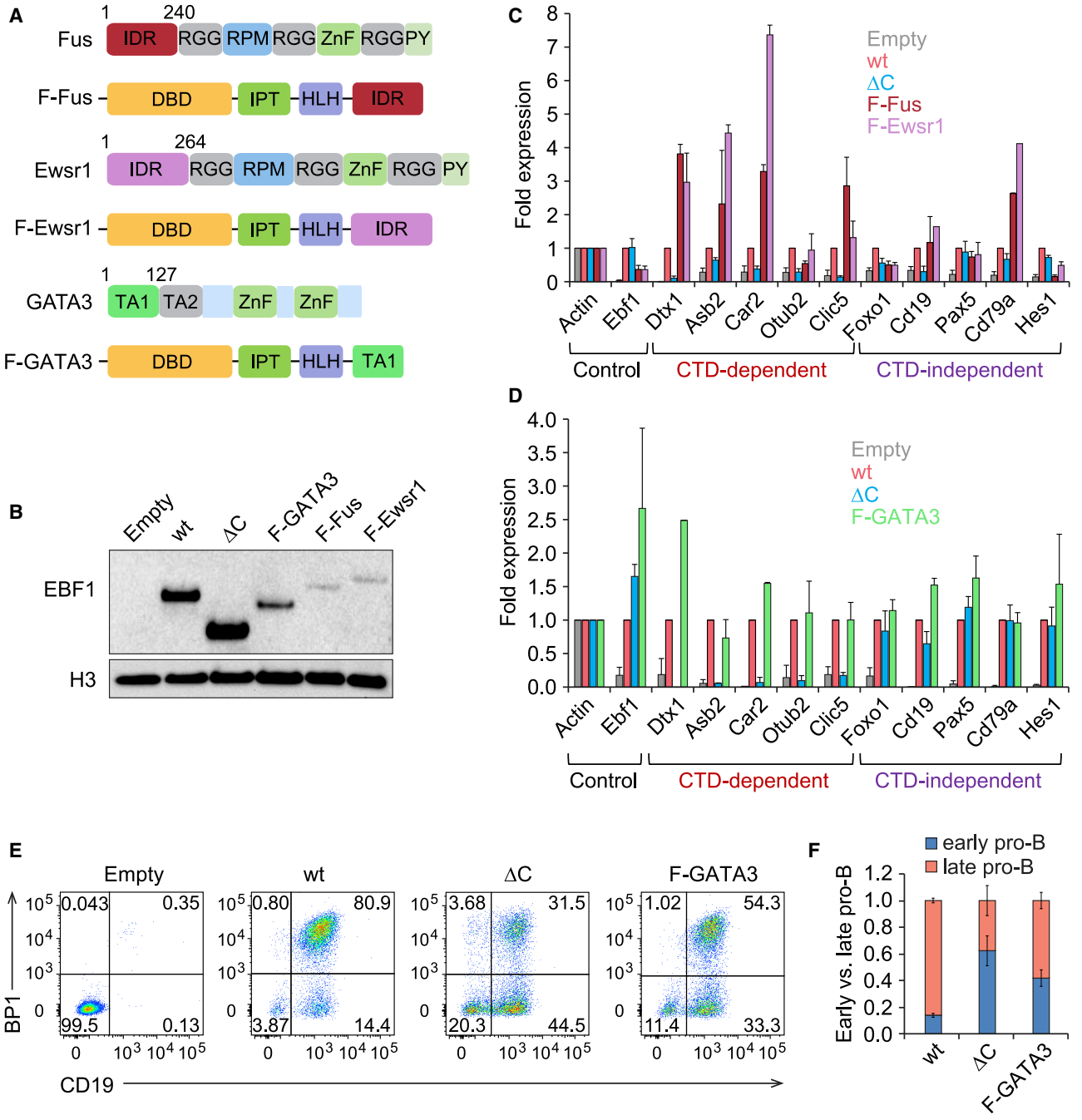

Figure 5. Heterologous Prion-like Domains Can Replace the C-Terminal Domain of EBF1

(A) Scheme of the fusion proteins. The N-terminal intrinsically disordered region of FUS or EWSR1 and the transactivation domain 1 (TA1) of GATA3 that were previously characterized as prion-like domains were fused to EBF1ΔC to generate the fusion proteins F-Fus, F-Ewsr1, and F-GATA3.

(B) Immunoblot analysis to detect the expression of EBF1wt, EBF1ΔC, and EBF1 fusion proteins by anti-EBF1 antibody. H3 is a loading control.

(C and D) qRT-PCR analysis to detect transcripts from control genes, CTD-dependent genes, and CTD-independent genes after 1 day of transduction (C) or 5 days of transduction (D). Raw cycle values were first normalized to actin and are represented as fold expression relative to EBF1wt-expressing cells. Error bars represent SD of three biological replicates.

(E) Representative flow cytometric analysis to detect BP1 and CD19 expression on GFP-positive cells that have been transduced with EBF1wt-, EBF1ΔC-, or EBF1ΔC-GATA3 fusion protein (F-GATA3)-expressing retroviruses 2 weeks prior to analysis. Percentages of $CD19^{+}BP1^{-}$ early pro-B and $CD19^{+}BP1^{+}$ late pro-B cells are indicated.

(F) Analysis of the ratio of early pro-B versus late pro-B. Error bars represent SD from three biological replicates.

Please cite this article in press as: Wang et al., A Prion-like Domain in Transcription Factor EBF1 Promotes Phase Separation and Enables B Cell Programming of Progenitor Chromatin, Immunity (2020), https://doi.org/10.1016/j.immuni.2020.10.009

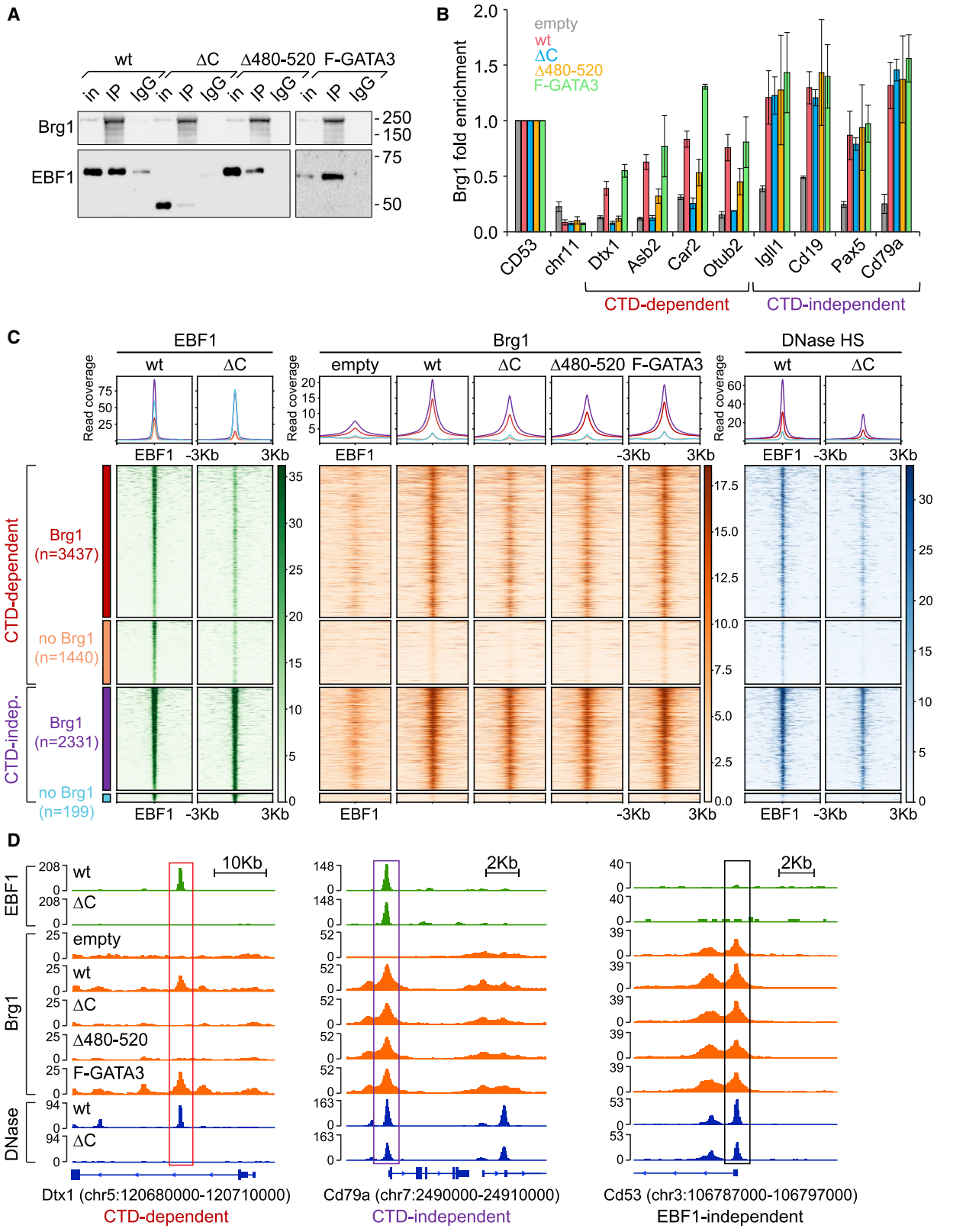

(legend on next page)

Please cite this article in press as: Wang et al., A Prion-like Domain in Transcription Factor EBF1 Promotes Phase Separation and Enables B Cell Programming of Progenitor Chromatin, Immunity (2020), https://doi.org/10.1016/j.immuni.2020.10.009

of Brg1 with EBF1Δ480-520 was reduced to a lesser extent than with EBF1ΔC, consistent with the partial removal of predicted IDR sequences in the Δ480-520 mutant (Figure S3B). Thus, the interaction of Brg1 with EBF1 involves the PLD in the CTD or a heterologous PLD.

To assess the genome-wide and gene-specific Brg1 occupancy in cells expressing wild-type or mutant EBF1, we performed ChIP-seq and quantitative ChIP analysis. The recruitment of Brg1 to EBF1-occupied sites was reduced in EBF1ΔC- and Δ480-520-expressing cells relative to EBF1wt- and F-GATA3-expressing cells (Figures 6B and 6C). In EBF1ΔC- and Δ480-520-expressing cells, the decrease in Brg1 occupancy at EBF1-bound sites was more pronounced at CTD-dependent sites than at CTD-independent sites (Figures 6B and 6C). As a control, similar Brg1 binding was observed at sites that did not overlap with EBF1 occupancy (Figures 6D and S6A). Gene-specific analysis showed that the binding of Brg1 at the CTD-dependent genes *Dtx1*, *Asb2*, *Car2*, and *Otub2* was severely impaired in EBF1ΔC-expressing cells relative to EBF1wt and F-GATA3-expressing cells (Figures 6B, 6D, and S6B). In contrast, we did not detect significant changes of Brg1 occupancy at the CTD-independent genes *Cd19*, *Igll1*, *Cd79a*, and *Pax5*. Likewise, the EBF1-independent Brg1 occupancy at the transcription start site of the *Cd53* gene was similar in the different samples (Figure 6D).

We have previously shown that a significant fraction of EBF1-occupied sites is not associated with the formation of DNase I hypersensitivity (Boller et al., 2016). Therefore, we also interrogated the EBF1 and Brg1 ChIP-seq datasets with a DNase I dataset. This analysis showed that 5,768 EBF1wt-occupied sites overlap with both Brg1 occupancy and DNase I hypersensitivity, whereas 1,639 EBF1wt-occupied sites that lack detectable Brg1 binding are not associated with DNase I hypersensitivity (Figures 6C). Thus, the CTD of EBF1 is required for the recruitment of Brg1, which correlates with the formation of chromatin accessibility at EBF1-occupied sites.

In conclusion, our experiments show that the chromatin opening at EBF1-bound regulatory sites in lymphoid progenitors involves distinct steps: (1) initial CTD-independent chromatin targeting by EBF1, (2) recruitment of Brg1 via the CTD of EBF1 or via adjacent transcription factors, and (3) EBF1-CTD-mediated phase transition and chromatin opening by Brg1 (Figure S6C). Although we have no direct evidence for a functional role of FET family proteins in EBF1-mediated B cell programming, this last step may involve EBF1-CTD-mediated and FUS-enhanced phase transition and a potential clustering of phase-separated chromatin domains.

DISCUSSION

Our data indicate that the B-lineage-pioneering of progenitor chromatin by EBF1 involves a PLD in its C terminus that mediates the interaction with RNA-binding proteins of the FET family and the recruitment of Brg1. The PLD of EBF1 also enabled liquid-liquid phase separation and the formation of condensates *in vitro* that underpins the appearance of dynamic puncta in nuclei. Finally, the PLD enabled EBF1 to activate a specific set of genes that is related to early events in lineage specification and has a limited co-occupancy by other transcription factors. Thus, we propose that EBF1-mediated Brg1 recruitment and phase separation underlie the pioneer function of EBF1 in B cell programming.

Our previous time-resolved analysis of chromatin binding by EBF1 indicated a sequential order of events, beginning with the binding of EBF1 at 6 h of induction, subsequent formation of chromatin accessibility and onset of gene expression at 24 h, and the loss of DNA methylation after 72 h (Li et al., 2018). A similar order of events was observed in a kinetic analysis of chromatin binding by the pioneer factor FoxA2 (Donaghey et al., 2018). Although FoxA2 is required for initiating chromatin opening, it depends on additional transcription factors and the BAF remodeling complex for generating accessible chromatin domains (Cernilogar et al., 2019; Lin et al., 2012). Pioneer transcription factors can bind their target sites in the context of nucleosomes, promote local opening of chromatin, and enable binding of other transcription factors (Iwafuchi-Doi and Zaret, 2016; Zaret and Carroll, 2011). Recent screening of transcription factors for their ability to bind nucleosomes *in vitro* indicated that short α helices that bind less than half of the circumference of nucleosomal DNA allow for strong binding (Garcia-Alonso et al., 2019; Zhu et al., 2018). In particular, short α helices found in FoxA3, Oct4; PU.1, and GATA3 have been associated with strong nucleosome binding capacity at nanomolar concentrations. In these screens, EBF proteins were not included and could not be compared with other pioneer factors. EBF1 also contains short DNA recognition helices, and it has an unusual mode of DNA recognition in which both half sites of the palindromic binding site are recognized by each monomer of the dimeric protein (Treiber et al., 2010a). *In vivo* analysis of nucleosome binding by pioneer factors suggested that pioneer factors

Figure 6. The Prion-like Domain Is Required for EBF1-Mediated Brg1 Recruitment at CTD-Dependent Sites

(A) Co-immunoprecipitation of Brg1 and EBF1 proteins from lysates of *Ebf1*$^{-/-}$ progenitor cells transduced with retroviruses expressing EBF1wt, EBF1ΔC, Δ480-520 (deletion of PLD), or F-GATA3 (fusion of the TA1 domain of GATA3 onto EBF1ΔC). Proteins were immunoprecipitated with anti-Brg1 antibody, and the immunoblots were probed with anti-Brg1 or anti-FLAG-HRP antibodies. In represents 2% input. IgG was used as a control.

(B) Quantitative ChIP analysis to detect Brg1 binding to CTD-dependent and -independent EBF1-sites in *Ebf1*$^{-/-}$ progenitor cells transduced with empty or EBF1-expressing retroviruses as described in (A). Brg1 binding was normalized to an EBF1-independent Brg1 site in the *Cd53* locus. An intergenic region on chromosome 11 (chr11) served as negative control. Error bars represent SD of three biological replicates.

(C) Heatmaps of ChIP-seq analysis to detect Brg1 occupancy in *Ebf1*$^{-/-}$ progenitor cells transduced with empty vector or EBF1-expressing vectors as described in (A). EBF1 occupancy and DNase hypersensitivity data were taken from Boller et al., 2016. Occupancy is shown ± 3 kb around EBF1 peak summits. EBF1 peaks are organized into four groups: CTD-dependent EBF1 peaks that overlap with Brg1 peaks (red); CTD-dependent EBF1 peaks with no Brg1 peak (pink); CTD-independent EBF1 peaks that overlap with Brg1 peak (purple); and CTD-independent EBF1 peaks with no Brg1 peak (blue). Peaks in all samples are ordered according to EBF1wt peaks. Heatmap scale represents read coverage. The average read coverage profiles are shown above the heatmaps.

(D) Occupancy profiles of EBF1 and Brg1 occupancy and DNase I hypersensitive sites in pro-B cells. Representative CTD-dependent *(Dtx1)*, CTD-independent *(Cd79a)*, and EBF1-independent *(Cd53)* genes are shown. The vertical axis represents read coverage.

initially access low-affinity motifs, thus enhancing the search space prior to stable binding in concert with other factors (Cernilogar et al., 2019; Meers et al., 2019).

The CTD of EBF1 is required for the activation of a specific set of genes that is involved in early lineage specification and contains regulatory regions in which EBF1 binds without extensive co-occupancy by other transcription factors (Boller et al., 2016). These findings raised the question of whether the CTD is generally involved in chromatin binding or reduces the need for collaboration with other transcription factors. Our current analysis of chromatin binding by EBF1ΔC at 6 h of induction indicated that the CTD is dispensable for an initial EBF1 targeting of both CTD-dependent and CTD-independent binding sites in the context of naive, unprogrammed progenitor chromatin. However, this initial chromatin targeting was not stable at CTD-dependent regulatory regions. Stable EBF1 binding at CTD-dependent sites was associated with the recruitment of Brg1, which interacts with the PLD as the functional determinant of the CTD.

Previous single-molecule tracking experiments showed that the pioneer factor FoxA1 has a relatively short (~9 s) residence time on DNA (Morisaki et al., 2014). According to the "dynamic assisted loading" model of pioneer factors, the recruitment of chromatin remodeling factors by pioneer factors and cooperation with other transcription factors are needed to stabilize binding by generating DNase I hypersensitive sites (Swinstead et al., 2016a, 2016b). Like EBF1, other pioneer factors including FoxA2, GATA3, Oct4, and steroid receptors interact with BAF or INO80 remodeling complexes to enable the generation of accessible chromatin regions (Hoffman et al., 2018; King and Klose, 2017; Takaku et al., 2016). Thus, the initial binding of pioneer transcription factors may be stabilized by the recruitment of remodeling complexes either via an intrinsic transcription factor domain or via other cooperating transcription factors. Similar to the ability of the CTD of EBF1, which enables chromatin binding in the absence of cooperating transcription factors, the TA1 domain of GATA3 is required for occupancy at a specific set of target sites (Takaku et al., 2016).

Our analysis also showed that a set of ~1,440 EBF1-bound sites is not associated with Brg1 binding and formation of chromatin accessibility. At these sites, stable EBF1 binding may involve nucleosome sliding rather than nucleosome eviction. We did not detect any significant differences in the sequences of EBF1-binding sites in the clusters with and without Brg1 recruitment (data not shown). However, EBF1-occupied sites that lack DNase I hypersensitivity are not associated with PU.1 and Pax5 co-occupancy, suggesting that a cooperation between EBF1 and other transcription factors enhances the recruitment of Brg1 and the formation of chromatin accessibility.

The observation that Brg1 recruitment coincided with EBF1 occupancy at 6 h of EBF1 induction is surprising, as chromatin accessibility is not yet detectable at this time point but is observed at 24 h of EBF1 induction (Li et al., 2018). This finding raises the question of which events occur between Brg1 recruitment and chromatin opening. The PLD of EBF1 is not only involved in the interaction with Brg1 but also confers phase separation ability upon EBF1. Moreover, the PLD is the functional unit of the CTD that enables EBF1 to activate CTD-dependent genes in progenitor cells. The PLD of EBF1 has several amino acid compositional features that resemble those found in FUS. In particular, the PLDs of both proteins have an array of evenly spaced tyrosine residues that are important for the phase separation ability of FUS (Chong et al., 2018; Kato et al., 2012). FUS phase separation involves cooperative cation-π interactions between tyrosines in the N-terminal PLD and arginines in a structured C-terminal domain, whereby arginine methylation modulates these interactions (Qamar et al., 2018; Wang et al., 2018). Notably, the phase separation ability of EBF1 was found to be enhanced *in vitro* by an interaction with FUS, a member of the FET family of RNA-binding proteins. Both FUS and EWSR1 have been shown to interact as oncogenic fusion proteins with Brg1 (Lindén et al., 2019). In oncogenic fusions of the PLD of EWSR1 to the DNA-binding domain of FLI1, Brg1 is recruited to GGAA repeats, which allows for aberrant chromatin opening (Boulay et al., 2017). Taken together, these data suggest a possible role of phase separation in the function of Brg1 in chromatin opening.

Liquid-liquid phase separation has also been implicated in the organization of chromatin (Gibson et al., 2019; Larson et al., 2017; Sanulli et al., 2019; Strom et al., 2017). In particular, the formation of heterochromatin by HP1α and Swi6 has been shown to involve inter- and intramolecular interactions that drive multivalent contacts and phase separation (Larson et al., 2017; Sanulli et al., 2019; Strom et al., 2017). Moreover, histone acetylation has been found to elicit dissolution of chromatin droplets and alter phase separation by multi-bromodomain proteins, including BRD4 (Gibson et al., 2019). Therefore, we propose a model in which Brg1 is recruited to EBF1-occupied regulatory sites via the CTD but requires phase separation for chromatin opening and clustering of EBF1-bound sites to facilitate the coordinate expression of EBF1 target genes. Our data suggest that EBF1-driven phase separation is especially important for the stable binding and function of EBF1 at CTD-dependent sites that lack the cooperation with other transcription factors. At CTD-independent sites, the requirement of the EBF1 CTD may be compensated by other transcription factors such as PU.1, which are expressed in *Ebf1*$^{-/-}$ progenitors and can bind chromatin as a pioneer factor without requiring accessibility (Heinz et al., 2010; Minderjahn et al., 2020; Ungerbäck et al., 2018). Interestingly, PU.1 has also been shown to affect transcription factor occupancy at a distance (Hosokawa et al., 2018).

Phase separation has also been implicated in transcriptional activation (Boija et al., 2018; Chong et al., 2018; Larson et al., 2017; Nair et al., 2019; Strom et al., 2017). In particular, transcription activation domains frequently contain low complexity regions that allow for compartmentalization by phase separation via the Mediator, which bridges transcription factors with RNA polymerase II, or via BRD4, which facilitates the release of RNA polymerase II from transcription start sites (Banani et al., 2017; Cho et al., 2018; Chong et al., 2018; Sabari et al., 2018; Wang et al., 2018). Notably, Med1 and BRD4 form distinct nuclear condensates, suggesting a specificity of homotypic self-interactions (Sabari et al., 2018). Likewise, FUS and Sp1 form distinct sub-nuclear puncta, suggesting that phase separation via homotypic interactions allows for the segregation of

proteins into distinct compartments (Chong et al., 2018). Although the phase separation property of EBF1 was not as pronounced as that of FET proteins, the CTD, and specifically the PLD of EBF1, enabled EBF1 to partition into phase-separated FUS condensates *in vitro*. Therefore, EBF1 may target not only Brg1 but also FET proteins to specific genomic sites, allowing for the coordination of chromatin opening, enhancer-promoter interactions, and the recruitment of the transcriptional activation machinery.

In conclusion, our data suggest that the programming of naive progenitor chromatin by EBF1 involves multiple steps that depend on the function of the C-terminal domain. Initial chromatin binding by EBF1 requires only the DNA-binding and dimerization domains. An additional short prion-like, low complexity domain in the C terminus of EBF1 mediates the recruitment of the Brg1 component of the BAF chromatin remodeling complex, which coincides with the initial EBF1 binding. The C-terminal domain also confers phase separation ability upon EBF1, which may be enhanced by FET family proteins and lead to Brg1-mediated chromatin opening, gene activation, and clustering of EBF1-occupied targets. Such stepwise programming of progenitor chromatin may ensure the correct and robust establishment of new gene programs during cell fate decisions.

Limitations of Study

One limitation of our study is the lack of a mechanistic connection between the CTD dependence of EBF1-mediated Brg1 recruitment, phase separation, and chromatin opening. The CTD of EBF1 confers phase separation on EBF1 and mediates the interaction with Brg1. However, the temporal sequence of molecular events such as Brg1 recruitment, EBF1 phase separation and chromatin opening, and the cause/consequence relationship between these events remain to be determined. Based on the partitioning of EBF1 into FUS condensates, we speculate that the EBF1-mediated phase separation is linked to the recruitment of FUS after the binding of EBF1 and Brg1 to chromatin. However, we have no evidence for a direct role of FET family proteins in EBF1-driven chromatin opening. FET family proteins seem to act redundantly (Boulay et al., 2017), and it will therefore be necessary to assess their roles in chromatin opening by combined conditional deletion or induced protein degradation. The imaging analysis of EBF1, Brg1, and FUS revealed a colocalization that is modestly but significantly reduced by the removal of the CTD. However, these proteins showed extensive expression throughout the nucleus, which complicated any mechanistic interpretation. Chromatin conformation analysis may provide insight into CTD-dependent clustering of EBF1 target genes. It will also be interesting to define the molecular grammar that confers phase separation ability upon EBF1. We are aware that much needs to be learned, but the link between EBF1 chromatin binding and phase separation ability opens many avenues toward exploring the biological significance of phase separation for chromatin opening and the coordination of lineage-specific gene expression.

STAR★METHODS

Detailed methods are provided in the online version of this paper and include the following:

SUPPLEMENTAL INFORMATION

Supplemental Information can be found online at https://doi.org/10.1016/j.immuni.2020.10.009.

ACKNOWLEDGMENTS

We are grateful to Drs. Anthony Hyman and Jie Wang (Max Planck Institute of Molecular Cell Biology and Genetics, Dresden) for generously providing plasmids and purified FUS protein. We thank Herbert Holzer (Asifa Akhtar lab) for technical help with protein expression in insect cells, Ingrid Falk for technical assistance, and Marika Rott for help in the manuscript preparation. We are grateful to Drs. Simon Alberti, Ritwick Sawarkar, and Eirini Trompouki for discussions and critical reading of the manuscript. We also thank members of the Grosschedl lab for discussions. This work was supported by funds from the Max Planck Society, Germany.

AUTHOR CONTRIBUTIONS

Conceptualization, funding acquisition, project coordination, and supervision, R.G. Retroviral transduction, FACS and FRAP analysis, phase separation assays, and imaging, Y.W. Co-immunoprecipitation, ChIP-seq analysis, and bioinformatic data analysis, N.Z. Cloning and retroviral transductions, C.-Y.Y. Imaging analysis, A.R. Mass spectrometry, G.M. Experimental design, Y.W., N.Z., and R.G. Paper writing, Y.W., N.Z., and R.G. Review and editing, all authors.

DECLARATION OF INTERESTS

The authors declare no competing interests.

Received: April 3, 2020
Revised: September 14, 2020
Accepted: October 14, 2020
Published: November 6, 2020

REFERENCES

Alberti, S., Gladfelter, A., and Mittag, T. (2019). Considerations and Challenges in Studying Liquid-Liquid Phase Separation and Biomolecular Condensates. Cell *176*, 419–434.

Bailey, T.L., and Machanick, P. (2012). Inferring direct DNA binding from ChIP-seq. Nucleic Acids Res. *40*, e128.

Banani, S.F., Lee, H.O., Hyman, A.A., and Rosen, M.K. (2017). Biomolecular condensates: organizers of cellular biochemistry. Nat. Rev. Mol. Cell Biol. *18*, 285–298.

Batista, C.R., Li, S.K., Xu, L.S., Solomon, L.A., and DeKoter, R.P. (2017). PU.1 regulates Ig light chain transcription and rearrangement in pre-B cells during B cell development. J. Immunol. *198*, 1565–1574.

Bhardwaj, V., Heyne, S., Sikora, K., Rabbani, L., Rauer, M., Kilpert, F., Richter, A.S., Ryan, D.P., and Manke, T. (2019). snakePipes: facilitating flexible, scalable and integrative epigenomic analysis. Bioinformatics *35*, 4757–4759.

Boija, A., Klein, I.A., Sabari, B.R., Dall'Agnese, A., Coffey, E.L., Zamudio, A.V., Li, C.H., Shrinivas, K., Manteiga, J.C., Hannett, N.M., et al. (2018). Transcription Factors Activate Genes through the Phase-Separation Capacity of Their Activation Domains. Cell *175*, 1842–1855.e16.

Boller, S., and Grosschedl, R. (2014). The regulatory network of B-cell differentiation: a focused view of early B-cell factor 1 function. Immunol. Rev. *261*, 102–115.

Boller, S., Ramamoorthy, S., Akbas, D., Nechanitzky, R., Burger, L., Murr, R., Schübeler, D., and Grosschedl, R. (2016). Pioneering Activity of the C-Terminal Domain of EBF1 Shapes the Chromatin Landscape for B Cell Programming. Immunity *44*, 527–541.

Bossen, C., Murre, C.S., Chang, A.N., Mansson, R., Rodewald, H.R., and Murre, C. (2015). The chromatin remodeler Brg1 activates enhancer repertoires to establish B cell identity and modulate cell growth. Nat. Immunol. *16*, 775–784.

Boulay, G., Sandoval, G.J., Riggi, N., Iyer, S., Buisson, R., Naigles, B., Awad, M.E., Rengarajan, S., Volorio, A., McBride, M.J., et al. (2017). Cancer-Specific Retargeting of BAF Complexes by a Prion-like Domain. Cell *171*, 163–178.19.

Carrero, G., McDonald, D., Crawford, E., de Vries, G., and Hendzel, M.J. (2003). Using FRAP and mathematical modeling to determine the in vivo kinetics of nuclear proteins. Methods *29*, 14–28.

Cernilogar, F.M., Hasenöder, S., Wang, Z., Scheibner, K., Burtscher, I., Sterr, M., Smialowski, P., Groh, S., Evenroed, I.M., Gilfillan, G.D., et al. (2019). Pre-marked chromatin and transcription factor co-binding shape the pioneering activity of Foxa2. Nucleic Acids Res. *47*, 9069–9086.

Cho, W.K., Spille, J.H., Hecht, M., Lee, C., Li, C., Grube, V., and Cisse, I.I. (2018). Mediator and RNA polymerase II clusters associate in transcription-dependent condensates. Science *361*, 412–415.

Choi, J., Ko, M., Jeon, S., Jeon, Y., Park, K., Lee, C., Lee, H., and Seong, R.H. (2012). The SWI/SNF-like BAF complex is essential for early B cell development. J. Immunol. *188*, 3791–3803.

Chong, S., Dugast-Darzacq, C., Liu, Z., Dong, P., Dailey, G.M., Cattoglio, C., Heckert, A., Banala, S., Lavis, L., Darzacq, X., and Tjian, R. (2018). Imaging dynamic and selective low-complexity domain interactions that control gene transcription. Science *361*, https://doi.org/10.1126/science.aar2555.

Donaghey, J., Thakurela, S., Charlton, J., Chen, J.S., Smith, Z.D., Gu, H., Pop, R., Clement, K., Stamenova, E.K., Karnik, R., et al. (2018). Genetic determinants and epigenetic effects of pioneer-factor occupancy. Nat. Genet. *50*, 250–258.

Gao, H., Lukin, K., Ramírez, J., Fields, S., Lopez, D., and Hagman, J. (2009). Opposing effects of SWI/SNF and Mi-2/NuRD chromatin remodeling complexes on epigenetic reprogramming by EBF and Pax5. Proc. Natl. Acad. Sci. USA *106*, 11258–11263.

Garcia-Alonso, L., Holland, C.H., Ibrahim, M.M., Turei, D., and Saez-Rodriguez, J. (2019). Benchmark and integration of resources for the estimation of human transcription factor activities. Genome Res. *29*, 1363–1375.

Georgopoulos, K. (2002). Haematopoietic cell-fate decisions, chromatin regulation and ikaros. Nat. Rev. Immunol. *2*, 162–174.

Gibson, B.A., Doolittle, L.K., Schneider, M.W.G., Jensen, L.E., Gamarra, N., Henry, L., Gerlich, D.W., Redding, S., and Rosen, M.K. (2019). Organization of Chromatin by Intrinsic and Regulated Phase Separation. Cell *179*, 470–484.e21.

Hagman, J.D. (1983). Presentation- and test-trial effects on acquisition and retention of distance and location. J. Exp. Psychol. Learn. Mem. Cogn. *9*, 334–345.

Hagman, J., Gutch, M.J., Lin, H., and Grosschedl, R. (1995). EBF contains a novel zinc coordination motif and multiple dimerization and transcriptional activation domains. EMBO J. *14*, 2907–2916.

Harrison, A.F., and Shorter, J. (2017). RNA-binding proteins with prion-like domains in health and disease. Biochem. J. *474*, 1417–1438.

Heinz, S., Benner, C., Spann, N., Bertolino, E., Lin, Y.C., Laslo, P., Cheng, J.X., Murre, C., Singh, H., and Glass, C.K. (2010). Simple combinations of lineage-determining transcription factors prime cis-regulatory elements required for macrophage and B cell identities. Mol. Cell *38*, 576–589.

Hoffman, J.A., Trotter, K.W., Ward, J.M., and Archer, T.K. (2018). BRG1 governs glucocorticoid receptor interactions with chromatin and pioneer factors across the genome. eLife *7*, e35073.

Hosokawa, H., Ungerbäck, J., Wang, X., Matsumoto, M., Nakayama, K.I., Cohen, S.M., Tanaka, T., and Rothenberg, E.V. (2018). Transcription Factor PU.1 Represses and Activates Gene Expression in Early T Cells by Redirecting Partner Transcription Factor Binding. Immunity *48*, 1119–1134.e7.

Hyman, A.A., Weber, C.A., and Jülicher, F. (2014). Liquid-liquid phase separation in biology. Annu. Rev. Cell Dev. Biol. *30*, 39–58.

Iwafuchi-Doi, M., and Zaret, K.S. (2016). Cell fate control by pioneer transcription factors. Development *143*, 1833–1837.

Kato, M., Han, T.W., Xie, S., Shi, K., Du, X., Wu, L.C., Mirzaei, H., Goldsmith, E.J., Longgood, J., Pei, J., et al. (2012). Cell-free formation of RNA granules: low complexity sequence domains form dynamic fibers within hydrogels. Cell *149*, 753–767.

King, H.W., and Klose, R.J. (2017). The pioneer factor OCT4 requires the chromatin remodeller BRG1 to support gene regulatory element function in mouse embryonic stem cells. eLife *6*, e22631.

Lancaster, A.K., Nutter-Upham, A., Lindquist, S., and King, O.D. (2014). PLAAC: a web and command-line application to identify proteins with prion-like amino acid composition. Bioinformatics *30*, 2501–2502.

Langmead, B., and Salzberg, S.L. (2012). Fast gapped-read alignment with Bowtie 2. Nat. Methods *9*, 357–359.

Larson, A.G., Elnatan, D., Keenen, M.M., Trnka, M.J., Johnston, J.B., Burlingame, A.L., Agard, D.A., Redding, S., and Narlikar, G.J. (2017). Liquid droplet formation by HP1α suggests a role for phase separation in heterochromatin. Nature *547*, 236–240.

Laslo, P., Spooner, C.J., Warmflash, A., Lancki, D.W., Lee, H.J., Sciammas, R., Gantner, B.N., Dinner, A.R., and Singh, H. (2006). Multilineage transcriptional priming and determination of alternate hematopoietic cell fates. Cell *126*, 755–766.

Li, H., Handsaker, B., Wysoker, A., Fennell, T., Ruan, J., Homer, N., Marth, G., Abecasis, G., and Durbin, R.; 1000 Genome Project Data Processing Subgroup (2009). The Sequence Alignment/Map format and SAMtools. Bioinformatics *25*, 2078–2079.

Li, R., Cauchy, P., Ramamoorthy, S., Boller, S., Chavez, L., and Grosschedl, R. (2018). Dynamic EBF1 occupancy directs sequential epigenetic and transcriptional events in B-cell programming. Genes Dev. *32*, 96–111.

Lin, H., and Grosschedl, R. (1995). Failure of B-cell differentiation in mice lacking the transcription factor EBF. Nature. https://doi.org/10.1038/376263a0.

Lin, Y.C., Jhunjhunwala, S., Benner, C., Heinz, S., Welinder, E., Mansson, R., Sigvardsson, M., Hagman, J., Espinoza, C.A., Dutkowski, J., et al. (2010). A global network of transcription factors, involving E2A, EBF1 and Foxo1, that orchestrates B cell fate. Nat. Immunol. *11*, 635–643.

Lin, Y.C., Benner, C., Mansson, R., Heinz, S., Miyazaki, K., Miyazaki, M., Chandra, V., Bossen, C., Glass, C.K., and Murre, C. (2012). Global changes in the nuclear positioning of genes and intra- and interdomain genomic interactions that orchestrate B cell fate. Nat. Immunol. *13*, 1196–1204.

Lin, Y., Protter, D.S., Rosen, M.K., and Parker, R. (2015). Formation and Maturation of Phase-Separated Liquid Droplets by RNA-Binding Proteins. Mol. Cell *60*, 208–219.

Lindén, M., Thomsen, C., Grundevik, P., Jonasson, E., Andersson, D., Runnberg, R., Dolatabadi, S., Vannas, C., Luna Santamaría, M., Fagman, H., et al. (2019). FET family fusion oncoproteins target the SWI/SNF chromatin remodeling complex. EMBO Rep. *20*, e45766.

Maier, H., Ostraat, R., Gao, H., Fields, S., Shinton, S.A., Medina, K.L., Ikawa, T., Murre, C., Singh, H., Hardy, R.R., and Hagman, J. (2004). Early B cell factor cooperates with Runx1 and mediates epigenetic changes associated with mb-1 transcription. Nat. Immunol. *5*, 1069–1077.

Malinovska, L., Kroschwald, S., and Alberti, S. (2013). Protein disorder, prion propensities, and self-organizing macromolecular collectives. Biochim. Biophys. Acta *1834*, 918–931.

Medina, K.L., Pongubala, J.M., Reddy, K.L., Lancki, D.W., Dekoter, R., Kieslinger, M., Grosschedl, R., and Singh, H. (2004). Assembling a gene regulatory network for specification of the B cell fate. Dev. Cell *7*, 607–617.

Meers, M.P., Janssens, D.H., and Henikoff, S. (2019). Pioneer Factor-Nucleosome Binding Events during Differentiation Are Motif Encoded. Mol. Cell *75*, 562–575.e5.

Mercer, E.M., Lin, Y.C., Benner, C., Jhunjhunwala, S., Dutkowski, J., Flores, M., Sigvardsson, M., Ideker, T., Glass, C.K., and Murre, C. (2011). Multilineage priming of enhancer repertoires precedes commitment to the B and myeloid cell lineages in hematopoietic progenitors. Immunity *35*, 413–425.

Minderjahn, J., Schmidt, A., Fuchs, A., Schill, R., Raithel, J., Babina, M., Schmidl, C., Gebhard, C., Schmidhofer, S., Mendes, K., et al. (2020). Mechanisms governing the pioneering and redistribution capabilities of the non-classical pioneer PU.1. Nat. Commun. *11*, 402.

Molliex, A., Temirov, J., Lee, J., Coughlin, M., Kanagaraj, A.P., Kim, H.J., Mittag, T., and Taylor, J.P. (2015). Phase separation by low complexity domains promotes stress granule assembly and drives pathological fibrillization. Cell *163*, 123–133.

Morisaki, T., Müller, W.G., Golob, N., Mazza, D., and McNally, J.G. (2014). Single-molecule analysis of transcription factor binding at transcription sites in live cells. Nat. Commun. *5*, 4456.

Nair, S.J., Yang, L., Meluzzi, D., Oh, S., Yang, F., Friedman, M.J., Wang, S., Suter, T., Alshareedah, I., Gamliel, A., et al. (2019). Phase separation of ligand-activated enhancers licenses cooperative chromosomal enhancer assembly. Nat. Struct. Mol. Biol. *26*, 193–203.

Nechanitzky, R., Akbas, D., Scherer, S., Györy, I., Hoyler, T., Ramamoorthy, S., Diefenbach, A., and Grosschedl, R. (2013). Transcription factor EBF1 is essential for the maintenance of B cell identity and prevention of alternative fates in committed cells. Nat. Immunol. *14*, 867–875.

Nutt, S.L., and Kee, B.L. (2007). The transcriptional regulation of B cell lineage commitment. Immunity *26*, 715–725.

Pongubala, J.M., Northrup, D.L., Lancki, D.W., Medina, K.L., Treiber, T., Bertolino, E., Thomas, M., Grosschedl, R., Allman, D., and Singh, H. (2008). Transcription factor EBF restricts alternative lineage options and promotes B cell fate commitment independently of Pax5. Nat. Immunol. *9*, 203–215.

Qamar, S., Wang, G., Randle, S.J., Ruggeri, F.S., Varela, J.A., Lin, J.Q., Phillips, E.C., Miyashita, A., Williams, D., Strohl, F., et al. (2018). FUS Phase Separation Is Modulated by a Molecular Chaperone and Methylation of Arginine Cation-pi Interactions. Cell *173*, 720–734.e15.

Quinlan, A.R. (2014). BEDTools: The Swiss-Army Tool for Genome Feature Analysis. Curr Protoc Bioinformatics *47*, https://doi.org/10.1002/0471250953.bi1112s47.

Ramírez, F., Ryan, D.P., Grüning, B., Bhardwaj, V., Kilpert, F., Richter, A.S., Heyne, S., Dündar, F., and Manke, T. (2016). deepTools2: a next generation web server for deep-sequencing data analysis. Nucleic Acids Res. *44*, https://doi.org/10.1093/nar/gkw257.

Ranganath, S., and Murphy, K.M. (2001). Structure and specificity of GATA proteins in Th2 development. Mol. Cell. Biol. *21*, 2716–2725.

Revilla-I-Domingo, R., Bilic, I., Vilagos, B., Tagoh, H., Ebert, A., Tamir, I.M., Smeenk, L., Trupke, J., Sommer, A., Jaritz, M., and Busslinger, M. (2012). The B-cell identity factor Pax5 regulates distinct transcriptional programmes in early and late B lymphopoiesis. EMBO J. *31*, 3130–3146.

Reynaud, D., Demarco, I.A., Reddy, K.L., Schjerven, H., Bertolino, E., Chen, Z., Smale, S.T., Winandy, S., and Singh, H. (2008). Regulation of B cell fate commitment and immunoglobulin heavy-chain gene rearrangements by Ikaros. Nat. Immunol. *9*, 927–936.

Rothenberg, E.V. (2014). Transcriptional control of early T and B cell developmental choices. Annu. Rev. Immunol. *32*, 283–321.

Sabari, B.R., Dall'Agnese, A., Boija, A., Klein, I.A., Coffey, E.L., Shrinivas, K., Abraham, B.J., Hannett, N.M., Zamudio, A.V., Manteiga, J.C., et al. (2018). Coactivator condensation at super-enhancers links phase separation and gene control. Science *361*, https://doi.org/10.1126/science.aar3958.

Sanulli, S., Trnka, M.J., Dharmarajan, V., Tibble, R.W., Pascal, B.D., Burlingame, A.L., Griffin, P.R., Gross, J.D., and Narlikar, G.J. (2019). HP1 reshapes nucleosome core to promote phase separation of heterochromatin. Nature *575*, 390–394.

Schwartz, J.C., Cech, T.R., and Parker, R.R. (2015). Biochemical Properties and Biological Functions of FET Proteins. Annu. Rev. Biochem. *84*, 355–379.

Strom, A.R., Emelyanov, A.V., Mir, M., Fyodorov, D.V., Darzacq, X., and Karpen, G.H. (2017). Phase separation drives heterochromatin domain formation. Nature *547*, 241–245.

Swinstead, E.E., Miranda, T.B., Paakinaho, V., Baek, S., Goldstein, I., Hawkins, M., Karpova, T.S., Ball, D., Mazza, D., Lavis, L.D., et al. (2016a). Steroid Receptors Reprogram FoxA1 Occupancy through Dynamic Chromatin Transitions. Cell *165*, 593–605.

Swinstead, E.E., Paakinaho, V., Presman, D.M., and Hager, G.L. (2016b). Pioneer factors and ATP-dependent chromatin remodeling factors interact dynamically: A new perspective: Multiple transcription factors can effect chromatin pioneer functions through dynamic interactions with ATP-dependent chromatin remodeling factors. BioEssays *38*, 1150–1157.

Takaku, M., Grimm, S.A., Shimbo, T., Perera, L., Menafra, R., Stunnenberg, H.G., Archer, T.K., Machida, S., Kurumizaka, H., and Wade, P.A. (2016). GATA3-dependent cellular reprogramming requires activation-domain dependent recruitment of a chromatin remodeler. Genome Biol. *17*, 36.

Thorvaldsdóttir, H., Robinson, J.T., and Mesirov, J.P. (2013). Integrative Genomics Viewer (IGV): high-performance genomics data visualization and exploration. Brief. Bioinform. *14*, 178–192.

Treiber, N., Treiber, T., Zocher, G., and Grosschedl, R. (2010a). Structure of an Ebf1:DNA complex reveals unusual DNA recognition and structural homology with Rel proteins. Genes Dev. *24*, 2270–2275.

Treiber, T., Mandel, E.M., Pott, S., Györy, I., Firner, S., Liu, E.T., and Grosschedl, R. (2010b). Early B cell factor 1 regulates B cell gene networks by activation, repression, and transcription- independent poising of chromatin. Immunity *32*, 714–725.

Ungerbäck, J., Hosokawa, H., Wang, X., Strid, T., Williams, B.A., Sigvardsson, M., and Rothenberg, E.V. (2018). Pioneering, chromatin remodeling, and epigenetic constraint in early T-cell gene regulation by SPI1 (PU.1). Genome Res. *28*, 1508–1519.

Wang, J., Choi, J.M., Holehouse, A.S., Lee, H.O., Zhang, X., Jahnel, M., Maharana, S., Lemaitre, R., Pozniakovsky, A., Drechsel, D., et al. (2018). A

Molecular Grammar Governing the Driving Forces for Phase Separation of Prion-like RNA Binding Proteins. Cell *174*, 688–699.e16.

Zandi, S., Mansson, R., Tsapogas, P., Zetterblad, J., Bryder, D., and Sigvardsson, M. (2008). EBF1 is essential for B-lineage priming and establishment of a transcription factor network in common lymphoid progenitors. J. Immunol. *181*, 3364–3372.

Zaret, K.S., and Carroll, J.S. (2011). Pioneer transcription factors: establishing competence for gene expression. Genes Dev. *25*, 2227–2241.

Zhang, Y., Liu, T., Meyer, C.A., Eeckhoute, J., Johnson, D.S., Bernstein, B.E., Nusbaum, C., Myers, R.M., Brown, M., Li, W., and Liu, X.S. (2008). Model-based analysis of ChIP-Seq (MACS). Genome Biol. *9*, R137.

Zhu, L.J., Gazin, C., Lawson, N.D., Pagès, H., Lin, S.M., Lapointe, D.S., and Green, M.R. (2010). ChIPpeakAnno: a Bioconductor package to annotate ChIP-seq and ChIP-chip data. BMC Bioinformatics *11*, 237.

Zhu, F., Farnung, L., Kaasinen, E., Sahu, B., Yin, Y., Wei, B., Dodonova, S.O., Nitta, K.R., Morgunova, E., Taipale, M., et al. (2018). The interaction landscape between transcription factors and the nucleosome. Nature *562*, 76–81.

Please cite this article in press as: Wang et al., A Prion-like Domain in Transcription Factor EBF1 Promotes Phase Separation and Enables B Cell Programming of Progenitor Chromatin, Immunity (2020), https://doi.org/10.1016/j.immuni.2020.10.009

STAR★METHODS

KEY RESOURCES TABLE

REAGENT or RESOURCE	SOURCE	IDENTIFIER
Antibodies		
α-EBF1 (1C), rabbit polyclonal	(Boller et al., 2016)	N/A
α-Brg1, rabbit monoclonal	Abcam	Cat# ab110641; RRID: AB_10861578
α-PU1, rabbit polyclonal	Santa Cruz	Cat# sc-352; RRID:AB_632289
α-FLAG M2-Peroxidase (HRP), mouse monoclonal	Sigma	Cat# A8592; RRID: AB_439702
α-H3, rabbit polyclonal	Abcam	Cat# ab1791; RRID: AB_302613
α-c-Kit biotin conjugated, rat monoclonal	BD PharMingen	Cat# 553353; RRID: AB_394804
α-mouse CD19 Violet421 conjugated, rat monoclonal	Biolegend	Cat# 115538; RRID: AB_11203527
α-BP1 PE conjugated, mouse monoclonal	BD pharmingen	Cat# 553735; RRID: AB_395018
α-HA tag, rat monoclonal	Roche	Cat# 11867423001; RRID: AB_390918
α-Flag, mouse monoclonal	Sigma	Cat# F3165; RRID: AB_259529
α-EWS, mouse monoclonal	Santa Cruze	Cat# sc-48404; RRID: AB_675525
α-FUS, mouse monoclonal	Santa Cruze	Cat# sc-47711; RRID: AB_2105208
α-FUS, rabbit polyclonal	Sigma-Aldrich	Cat# HPA008784; RRID: AB_1849181
anti-rabbit IgG Alexa Fluor-488, goat	Invitrogen	Cat# A-11034; RRID: AB_2576217
anti-mouse IgG Alexa Fluor-568, goat	Invitrogen	Cat# A-21124; RRID:AB_141611
anti-rat IgG Alexa Fluor-647, chicken	Invitrogen	Cat# A-21472; RRID:AB_2535875
α-EBF1 (6G6), rat monoclonal	E. Kremmer	N/A
Chemicals, Peptides, and Recombinant Proteins		
Puromycin	GIBCO	A11138-03
Doxycycline	Sigma	D9891
Ethylene glycol-bis(succinic acid N-hydroxysuccinimide ester) EGS	Sigma	E3257
SNAP-Surface Alexa Fluor 546	NEB	S9132S
RED-Tris-NTA	NanoTemper	MO-L018
1,6-hexanediol	Sigma-Aldrich	240117
Amylose resin	NEB	E8021S
EBF1 461-520 peptideNSSSVSPHGYVPSTTPQQTNYN SVTTSMNGYGSAAMSNLGGSPTFLNGSAANSPYAIVPS	BIOSYNTAN	N/A
EBF1 532-591 peptideSNCSSSSGIFSFSPANMVSAVK QKSAFAPVVRPQTSPPPTCTSTNGNSLQAISGMIVPPM	BIOSYNTAN	N/A
SNAP-FUS protein	(Wang et al., 2018)	N/A
His-BRG1 protein	Abcam	ab82237
MBP-EGFP protein	This study	N/A
MBP-EGFP-EBF1wt protein	This study	N/A
MBP-EGFP-EBF1ΔC protein	This study	N/A
Critical Commercial Assays		
NEBNext Ultra II DNA Library Prep Kit for Illumina	New England Biolabs	E7645L
Deposited Data		
α-Brg1 ChIP-seq in transduced pro-B cells	This study	GEO: GSE145991
α-Brg1 ChIP-seq in pro-B cells	(Bossen et al., 2015)	GEO: GSM1635413
α-EBF1 ChIP-seq in EBF1wt in pro-B cells	(Boller et al., 2016)	GEO: GSM2086725 GEO: GSM2086726
α-EBF1 ChIP-seq in EBF1ΔC-expressing pro-B cells	(Boller et al., 2016)	GEO: GSM2086732
DNase HS in EBF1wt-expressing pro-B cells	(Boller et al., 2016)	GEO: GSM2086730
DNase HS in EBF1ΔC-expressing pro-B cells	(Boller et al., 2016)	GEO: GSM2086731

(*Continued on next page*)

Please cite this article in press as: Wang et al., A Prion-like Domain in Transcription Factor EBF1 Promotes Phase Separation and Enables B Cell Programming of Progenitor Chromatin, Immunity (2020), https://doi.org/10.1016/j.immuni.2020.10.009

Continued

REAGENT or RESOURCE	SOURCE	IDENTIFIER
PU.1 ChIP-seq in pro-B cells	(Batista et al., 2017)	GEO: GSE87314
Experimental Models: Cell Lines		
AMuLV-transformed pro-B cells	(Boller et al., 2016)	N/A
Experimental Models: Organisms/Strains		
Mouse: *Ebf1*$^{+/-}$ C57BL/6	(Lin and Grosschedl, 1995)	N/A
Oligonucleotides		
Cloning primers	Table S1	N/A
qPCR primers	Table S2	N/A
Recombinant DNA		
pRetroX-Tight-Pur	Clontech	PT3960-5
Ewsr1 Mouse cDNA	OriGene	MR209810
FUS Mouse cDNA	OriGene	MR208306
Ebf1 mutant construct primers	Table S3	N/A
Software and Algorithms		
bowtie2 (v2.3.3.1)	(Langmead and Salzberg, 2012)	http://bowtie-bio.sourceforge.net/bowtie2/index.shtml RRID:SCR_005476
samtools (v1.9)	(Li et al., 2009)	http://www.htslib.org/RRID:SCR_002105
picard tools (v2.9.2)	N/A	https://broadinstitute.github.io/picard/ RRID: SCR_006525
deeptools (v3.3.1)	(Ramírez et al., 2016)	https://deeptools.readthedocs.io/en/develop/ RRID: SCR_016366
MACS2 (v2.1.2)	(Zhang et al., 2008)	https://github.com/macs3-project/MACS RRID: SCR_013291
ChIPpeakAnno (v3.16.0)	(Zhu et al., 2010)	https://www.bioconductor.org/packages/release/bioc/html/ChIPpeakAnno.html RRID: SCR_012828
bedtools2 (v2.27.0)	(Quinlan 2014)	https://bedtools.readthedocs.io/en/latest/content/installation.html RRID: SCR_006646
CentriMo (v4.11.1)	(Bailey and Machanick, 2012)	http://meme-suite.org/doc/centrimo.html RRID: SCR_001783
IGV genome browser	(Thorvaldsdóttir et al., 2013)	http://software.broadinstitute.org/software/igv/ RRID: SCR_011793
PLAAC algorithm	(Lancaster et al., 2014)	http://plaac.wi.mit.edu/
ZEN	ZEISS	https://www.zeiss.com/microscopy/int/products/microscope-software/zen.html RRID: SCR_018163
Imaris	Bitplane	https://imaris.oxinst.com/packages RRID: SCR_007370
esayFRAP	Cell Cycle Laboratory	https://easyfrap.vmnet.upatras.gr/

RESOURCE AVAILABILITY

Lead Contact

Further information and requests for resources and reagents should be directed to and will be fulfilled by the Lead Contact, Rudolf Grosschedl (grosschedl@ie-freiburg.mpg.de).

Materials Availability

The plasmids and anti-EBF1 antibodies used in this study can be obtained (pending continued availability) from the Lead Contact with a completed Materials Transfer Agreement.

Please cite this article in press as: Wang et al., A Prion-like Domain in Transcription Factor EBF1 Promotes Phase Separation and Enables B Cell Programming of Progenitor Chromatin, Immunity (2020), https://doi.org/10.1016/j.immuni.2020.10.009

Data and Code Availability

The ChIP-seq data reported in this paper are available in the Gene Expression Omnibus public database under the accession number GEO: GSE145991. Accession codes for PU.1 ChIP-seq data in pro-B cells (Batista et al., 2017) can be found in the referenced paper. Data of the imaging analysis are available upon request.

EXPERIMENTAL MODEL AND SUBJECT DETAILS

Mice

To obtain *Ebf1*$^{-/-}$ fetal liver cells, heterozygous *Ebf1*$^{-/+}$ (C57/BL6) mice were bred. E16.5-E17.5 embryos were genotyped and *Ebf1*$^{-/-}$ fetal livers were dispersed and combined for the isolation of cKit^{+} progenitors by Magnetic Activated Cell Sorting (MACS).

METHOD DETAILS

Transduction of fetal liver cells

EBF1-expressing GFP-bicistronic retroviruses were generated by transforming PlatE cells with the corresponding plasmids and by using the FuGene (Promega) reagent. For retroviral transduction, cKit-positive cells were MACS-sorted from dispersed *Ebf1*$^{-/-}$ fetal livers according to a standard protocol (Miltenyi Biotec). Fetal livers cells were transduced by spin infection (centrifugation 3000 g at 25°) with virus-containing supernatant and polybrene (8 μg/mL). 48 h after transduction, GFP-positive cells were sorted by flow cytometry and cultured on OP9 feeder cells in Opti-MEM medium for 7 days.

Generation of "Tet-On" cells

Cells for "Tet-On" induction were generated by sequential transduction of cKit-positive *Ebf1*$^{-/-}$ fetal liver cells with pMYS-Tet-On-Adv and pRetroX-Tight-Pur-EBF1wt- or EBF1ΔC-expressing retroviruses (Li et al., 2018). After selection, cells were cultured on OP9 feeder cells in Opti-MEM medium and cultured 14-20 days to obtain enough cells for analysis.

Transfection of HEK293T cells

HEK293T cells were plated at ~30% confluence one day before transfection. 20 μg of DNA was dissolved in 500 μL of a 250mM calcium chloride solution. Equal volume of 2x HBS buffer were added to the reaction and mixed by bubbling pipetting. The mixture was incubated at room temperature for 20 min and added dropwise to the cells. The cells were incubated at 37°C and 5% CO_2 for at least 6 h or overnight. Fresh medium was added to the cells. After 24 to 48 h the cells were collected for pulldown assays.

Molecular cloning

The pMys-IRES-GFP retroviral vector was used as a backbone vector to express EBF1 proteins. GFP-bicistronic EBF1wt and EBF1ΔC retroviral constructs have been described (Boller et al., 2016). C-terminal truncations were obtained by introducing stop codons at different amino acid positions via site-directed mutagenesis. For the generation of Fusion mutants, a SphI and MfeI cutting site was introduced into the Ebf1wt construct at position 422 and 591, respectively. The CTD fragment of EBF1 between positions 422 and 591 was subsequently replaced with different sequences as SphI/MfeI fragments. Primers used for cloning are indicated in Table S1. Gene constructs used in this study are listed in Table S3.

Quantitative RT-PCR

GFP and CD19 double positive cells were sorted and subjected to RNA extraction, using Trizol reagent (Life technologies). RNA was reverse transcribed into cDNA with Super Script II reverse transcriptase kit (Invitrogen). qRT-PCR analysis was performed with FAST SYBR Green Master Mix (Applied Biosystems). Primers used for qRT-PCR are listed in Table S2.

Flow cytometry (FACS)

For flow cytometry, single cell suspensions were treated with anti-CD16/32 (eBioscience) blocking antibody and stained with Violet421-conjugated anti-CD19 (Biolegend) and PE-conjugated anti-BP1 (BD PharMingen). Analytic flow cytometry of single cell suspensions was performed with BD LSR II. Data were analyzed with the FlowJo-software.

Peptide pulldown

Corresponding EBF1 peptides were crosslinked with Dynabeads M280 streptavidin (Invitrogen). Peptide-beads pulldowns were performed in nuclear extracts from SILAC-labeled 38B9 pro-B cells and subjected to mass spectrometry analysis.

Protein expression and purification

The insect cell line SF9 was used to express EBF1 proteins. Actively dividing SF9 cells were transfected with gene constructs for the expression of EBF1wt and mutant EBF1. After 72 h incubation at 27°C in SpodoPAN medium without serum and antibiotic, the supernatant was collected as virus P0. Virus P0 was used to infect SF9 cells and after 48 h to 72 h, the cells were harvested and lysed with buffer A(50mM Tris-HCl pH7.4; 500mM NaCl; 0.1% NP40; 1mM EDTA; 1mM DTT; 5% Glycerol; 5ug/mL Aprotinin; 5ug/mL Bestatin; 5ug/mL Antipain; 5ug/mL Trypsin/Chymotrypsin inhibitor; 5ug/mL Leupeptin; 2.5ug/mL Pepstatin). The cell lysate was

sonicated with a Branson sonifier 450 (3 cycles of 30 s on, 30 s off; output control 5 and duty cycle 20%) and spun down at 4000rpm 4°C for 30 min. Amylose resin was added to the cell lysate supernatant. The elution was carried out in overhead rotator at cold room overnight with elution buffer (buffer A plus 20mM maltose). The protein solution was collected and snap frozen by liquid nitrogen and stored at −80°C for later use.

In vitro phase separation assays

Recombinant GFP-EBF1wt and GFP-EBF1ΔC proteins were concentrated using Amicon Ultra centrifugal filters (10K and 50K MWCO, Millipore). The concentrated proteins were diluted in 50mM Tris-HCl pH7.4, 1mM EDTA, 1mM DTT, 0.1% NP40, 5% Glycerol to yield solutions at different concentrations and varying salt concentrations. The protein solution was immediately loaded to chamber of 15 μL slide (18-well flat from Ibidi) and analyzed under the Airyscan detector on an LSM880 confocal microscope (Zeiss). The images were taken under 63x oil objective at room temperature. Software ZEN black was used for data acquisition. Images were processed with ZEN and Imaris.

To assess phase separation by a turbidity assay, the recombinant GFP-EBF1 fusion proteins were mixed with an equal volume of 30% dextran, yielding a protein solution with 15% dextran. 15 μL of the protein mixture were loaded on an 18-well slide (Ibidi #81826) and incubated at room temperature for 10 min. Images of the 18-well flat slide were taken with Olympus SZ-30MR camera and Airyscan detector on an LSM880 confocal microscope (Zeiss).

For phase separation assays, SNAP-tagged FUS protein (kindly provided by J. Wang and A. Hyman, MPI Dresden) was mixed with SNAP-Surface Alexa Fluor 546 (S9132S NEB) at the ratio of 10:1 at room temperature for 5min. The mixture was centrifuged at 13000 g for 2min and the supernatant was used for experiments. Fluorescently labeled FUS protein was used alone or mixed with MBP-GFP-EBF1 or His-Brg1 (labeled with Kit RED-tris-NTA) in the presence of 5% dextran. The mixed protein solutions were loaded to chamber of 18-well flat slides and incubated at room temperature for 10 min. Recombinant His-tagged Brg1 protein was mixed with Monolith His-Tag Labeling Kit RED-Tris-NTA 2nd Generation (MO-L018 NanoTemper) at the ratio of 4:1. The mixed protein solution was incubated at room temperature for 30 min and centrifuged at 13 000 g and 4°C for 10 min. The supernatant was transferred to a fresh tube and used for experiments. Images were taken with the Airyscan detector on an LSM880 confocal microscope (Zeiss).

Fluorescence recovery after photobleaching

8-well chamber coverslips were prepared for attachment of cells with Corning® Cell-Tak Cell and Tissue Adhesive (2.05 mg/mL), according to the protocol of the manufacturer. 10^5 cells in 200 μL medium without serum were placed into each chamber and incubated at 37°C and 5% CO2 for 5 min. TOKAI HIT microscope stage top incubator as used for live cell imaging. Fluorescence recovery after photobleaching (FRAP) experiments were performed with Airyscan 880 confocal microscope using a 63× objective (oil immersion). Two different settings were used for FRAP experiments, FAST mode setting and LSM mode setting. For FAST mode, a region of 1.44 μm^2 was chosen and bleached with ten repetitions of the 514 argon laser and 561nm laser full laser power. Recovery was imaged with 2% laser power and 500 frames were recorded with Airyscan FAST mode (~1 frame/ms). For LSM mode, an EBF1 puncta was chosen and bleached with three repetitions of 561nm laser full laser power. Recovery was imaged with 2% laser power and frames were recorded every 4 s with Airyscan LSM mode. Pictures were analyzed with ZEN and the full-scale recovery intensity normalization was performed with easyFRAP (https://easyfrap.vmnet.upatras.gr/).

Treatment of cells with 1,6-hexanediol

Cells were attached to an 8-well slide as described above. 5% 1,6-hexanediol (Hex) in PBS was used to treat cells for 30 s. Cells were washed twice with PBS an immunofluorescence staining was performed according to the standart protocol.

Immunofluorescence staining

Cells were prepared on 8-well slides as described above. The liquid was aspirated and 200 μL 4% PFA was placed to each chamber. After fixation at RT for 10 min, the cells were washed three times with PBS plus 0.1% Triton (0.1% PBST). 0.5% Triton in PBS (0.5% PBST) was used to permeabilize cells at RT for 10min. Slides were blocked with 5% milk in 0.1% PBST for 10 min. Primary antibodies were used at 1 or 2 μg/mL and incubated at 4°C overnight. Alexa Fluor-conjugated secondary antibodies, diluted 1:200 with 5% milk in 0.1%PBST was applied to cells for 1 h at room temperature in dark. The cells were washed three times for 5 min with 0.1% PBST. 5 μg/mL DAPI or 10 μg/mL Hochest 33342 was used for nuclear staining at room temperature in the dark for 30 min. The cells were rinsed three times with PBS. Mounting medium was dropwise applied to cover the entire chamber. Anti-EBF1 rat monoclonal antibody (6G6, Helmholtz Center), anti-BRG1 rabbit antibody (ab110641, Abcam) and anti-FUS mouse antibody (sc-47711, Santa Cruz) were used for staining of 38B9 pro-B cells. Alexa Fluor-647 chicken anti-rat IgG(1812312, Invitrogen), Alexa Fluor-488 goat anti-rabbit IgG(A11034, Invitrogen) and Alexa Fluor-568 goat anti-mouse IgG(1081654, Invitrogen) were used to visualize EBF1, Brg1 and FUS, respectively. Anti-BRG1 rabbit antibody (ab110641, Abcam) or anti-FUS rabbit antibody (HPA008784, Sigma-Aldrich) were used for staining retrovirally transduced *Ebf1*$^{-/-}$ pre-pro-B cells. Alexa Fluor-488 goat anti-rabbit IgG secondary antibody (A11034, Invitrogen) was used to visualize Brg1 and FUS.

Please cite this article in press as: Wang et al., A Prion-like Domain in Transcription Factor EBF1 Promotes Phase Separation and Enables B Cell Programming of Progenitor Chromatin, Immunity (2020), https://doi.org/10.1016/j.immuni.2020.10.009

Image acquisition and analysis

The images were taken under Airyscan 880 confocal microscope using a 63× oil objective at room temperature. Software ZEN black was used for acquisition. 5-7 μm Z stack images were taken with intervals of 0.15 μm. Imaris 3D coloc wizard was used to analyze the colocalization by calculating the Pearson's coefficient in colocalized region.

Protein and immunoblot analysis

Protein gels were stained with 15 to 20ml InstantBlue (Expedeon) for 5 to 10 min without the need to wash, fix or destain. For immunoblot analysis, the proteins in the gels were transferred onto a nitrocellulose membrane. The membrane was incubated in 5% milk in PBS for 1 h and primary antibody in milk was added. After three washes with PBS and 0.1% Triton X-100, the secondary horse radish peroxidase-conjugated antibody was added. SuperSignal™ West Pico Plus chemiluminescent substrate or Femto Maximum Sensitivity substrate were used to visualize the proteins. Images were acquired with the ChemiDoc Touch Imaging system (Bio-Rad).

Co-immunoprecipitation

Cells were harvested and washed with PBS. Cell pellets were re-suspended in 1 mL IP-buffer (20 mM HEPES pH 7.6, 150 mM NaCl, 2 mM MgCl2, 0.1% (v/v) NP-40, 10% glycerol, protease inhibitor mix (PIM) and 1 mM PMSF). Cells were sonicated to disrupt nuclei (duty cycle 50%; output level 1.5; 2 × 10 cycles). For coimmunoprecipitations, 0.5 μg α-Brg1 antibody or rabbit IgG were used. Lysates were incubated on a rotator overnight at 4°C. Lysates were incubated with 20 μL Protein G Dynabeads (ThermoFisher Scientific) and 1% BSA on rotator for 3 h at 4°C. Beads were washed 4 times with 1 mL IP-buffer on rotator for 2 min at 4°C. Proteins were eluted with 1x SDS-PAGE loading buffer for 10 min at 95°C.

Induction of EBF1 expression

"Tet-On" induction of EBF1wt and EBF1ΔC expression in *Ebf1*$^{-/-}$ progenitor cells was performed according to the protocol described in Li et al., 2018. The medium was replaced with Opti-MEM medium containing 500 ng/mL doxycycline (Dox). Cells were incubated with Dox for 6 h. Human Bjab B cells were used as a spike-in control for Tet-On EBF1 ChIP experiments in a ratio of 1:10 (Bjab:Tet-On). All subsequent procedures were performed according to the standard EBF1 or Brg1 ChIP protocol.

EBF1 and PU.1 chromatin immunoprecipitations

EBF1 and PU.1 chromatin immunoprecipitations (ChIP) were performed according to the protocol of Boller et al., 2016 with the some changes. Only crosslinking with formaldehyde was used. 4 μg rabbit a-EBF1 (1C) rabbit antibody or 4 μg rabbit a-PU.1 antibody per sample was used. Cells were harvested and washed with PBS. The cell pellet was re-suspended in PBS with 2% FCS (4 x10^6 cells per 1 mL buffer). Fresh formaldehyde mix (50mM HEPES-KOH pH8.0, 100mM NaCl, 0.5mM EGTA, 1mM EDTA, 11% (v/v) formaldehyde) was added to the cell suspension to a final concentration of 1% FA. Tubes were incubated on rotator for 10 min at RT. Quenching was performed by adding 2 M Glycine to the final concentration 0.2 M. The cell pellet was re-suspended in lysis buffer (50mM Tris-HCl pH 8.0, 1% (w/v) SDS, 10mM EDTA; PIM) (4 x10^6 cells per 100 μL buffer). Chromatin was sheared the chromatin with a Bioruptor (20-25 cycles, output level "High," 30 s ON, 30 s OFF, 4°C). 10-20 μg DNA was used for 1 ChIP reaction. Chromatin was mixed with 4 μg of EBF1 antibody or rabbit IgG and incubated on rotator ON at 4°C. Chromatin was incubated with 30 μL of Dynabeads Protein G (ThermoFisherScientific) suspension per sample on rotator for 4 h at 4°C. Beads were washed 4 times with Wash buffer A (20mM Tris-HCl pH 8.0, 150mM NaCl, 1% (v/v) Triton X-100, 0.1% (w/v) SDS, 2mM EDTA); once with Final wash buffer A (20mM Tris-HCl pH 8.0, 500mM NaCl, 1% (v/v) Triton X-100, 0.1% (w/v) SDS, 2mM EDTA). Every wash was on rotator for 5 min at 4°C. Chromatin was eluted with 100 μL Elution buffer (10 mM Tris-HCl, pH 8.0; 0.5% SDS; 300 mM NaCl; 5 mM EDTA pH 8.0) by shaking vigorously at 65°C for 30 min. Samples were reverse crosslinked, treated with RNase A, Proteinase K, and purified with QIAquick PCR Purification Kit.

Brg1 chromatin immunoprecipitation

Brg1 ChIP was performed according to the protocol of Bossen et al., 2015 with the following changes. Double crosslinking with EGS and formaldehyde was used. 2.5 μg a-Brg1 antibody from Abcam (ab110641) per sample was used. Cells were harvested and washed with PBS. Cell pellets were re-suspended in 10-20 mL PBS. EGS stock solution in DMSO (150 mM - 0.0686 g/mL) was added 1:100 to the cell suspension. Tubes were incubated on a rotator for 15 min at RT. 37% formaldehyde stock solution was added to the final concentration 1%–2%. Tubes were incubated on a rotator for 15 min at RT. Quenching was performed by adding 2M Glycine to the final concentration 0.2 M. Cells were re-suspended in 4 mL buffer LB1 (50mM HEPES-KOH, pH 7.5; 140mM NaCl, 1mM EDTA; 10% glycerol; 0.5%NP-40; 0.25%Triton X-100; protease inhibitor mix (PIM) and incubated on ice for 10 min. Cells were re-suspended LB3 buffer (10mM Tris-HCl, pH 8.0; 200mM NaCl; 1mM EDTA, pH 8.0; 0.5mM EGTA, pH 8.0; 0.1%Na-Deoxycholate; 0.5% N-lauroylsarcosine; PIM) about 1.5-3 x10^6 cells per 100 μL buffer. Chromatin was sheared with a Bioruptor (20-25 cycles, output level "High," 30 s ON, 30 s OFF, 4°C). Fragment sizes and amounts of chromatin were analyzed. 30 μL of Dynabeads Protein G (ThermoFisherScientific) suspension per sample was coupled with 2.5 μg of Brg1 antibody or rabbit IgG in 200 μL of PBS with 0.5% BSA. 10-20 μg DNA was used for 1 ChIP reaction. Chromatin was added to beads and incubated on rotator ON at 4°C. Beads were washed with WB I (50 mM Tris-HCl, pH 8.0; 150 mM NaCl; 0.1% SDS; 0.1% NaDOC; 1% Triton X-100; 1 mM EDTA pH 8.0); WB II (50 mM Tris-HCl, pH 8.0; 500 mM NaCl; 0.1% SDS; 0.1% NaDOC; 1% Triton X-100; 1 mM EDTA pH 8.0); WB III (10 mM Tris-HCl, pH 8.0; 250 mM LiCl; 0.5% NP-40; 0.5% NaDOC; 1 mM EDTA pH 8.0) and TE. Every wash was on rotator for 5 min at 4°C. Chromatin was

Please cite this article in press as: Wang et al., A Prion-like Domain in Transcription Factor EBF1 Promotes Phase Separation and Enables B Cell Programming of Progenitor Chromatin, Immunity (2020), https://doi.org/10.1016/j.immuni.2020.10.009

eluted with 100 μL Elution buffer (10 mM Tris-HCl, pH 8.0; 0.5% SDS; 300 mM NaCl; 5 mM EDTA pH 8.0) by shaking vigorously at 65°C for 30 min. Samples were reverse cross-linked, treated with RNase A and Proteinase K, and purified with QIAquick PCR Purification Kit.

Quantitative PCR (qPCR)

qPCR after ChIP was performed according to standard protocol for Fast SYBR Green Master Mix (Thermo Fisher) on StepOnePlus qPCR machine. A standard curve was used for quantification. Primers used for ChIP-qPCR are listed in Table S2. For Brg1 ChIP normalization, all values were divided to CD53 value in each sample. For spike-in ChIP normalization, we first calculated the scaling coefficient as a ratio between the average input values for mouse and human targets. Subsequently, the hCD79b sample was adjusted using this coefficient. All samples were normalized to this adjusted spike-in value.

Library QC and Sequencing

ChIP-seq library preparation was performed with the NEBNext Ultra II DNA Prep library Kit (Illumina). Amplifications involved 10-12 PCR cycles. No size selection was used. Before sequencing, libraries were quantified by qPCR, and the size distribution was assessed using Fragment analyzer. Deep sequencing was performed on HiSeq 3000 according to the standard protocol for 75bp or 100bp paired-end reads.

QUANTIFICATION AND STATISTICAL ANALYSIS

In all figures and legends, the mean and standard deviations (SD) are indicated. The numbers of biological replications are described in the figure legends. p values were calculated by unpaired t test.

In vitro phase separation

Phase separation images were analyzed with Imaris Surface function. All phase-separated droplets were selected and a mask was applied. Fluorescence intensity was measured in the masked area, using the same setting for all images. The relative amounts of condensed EBF1wt and EBF1ΔC proteins were determined by normalizing fluorescence intensity at different concentrations to that of EBF1wt at 10 μM.

Image analysis

FRAP analysis: Images were analyzed with ZEN and the full-scale recovery intensity normalization was performed with easyFRAP (https://easyfrap.vmnet.upatras.gr/).

Colocalization analysis: The Imaris 3D coloc wizard was used to determine the colocalization by calculating the Pearson's coefficient in colocalized regions.

Quantification of EBF1 puncta: Spots-creation wizard from Imaris was used to automatically detect point-like structures. The settings for automatically detected spot-diameters were 0.2 μm, 0.25 μm and 0.3 μm.

ChIP-seq analysis

Automatic pipeline for analysis of deep sequencing data was used (Bhardwaj et al., 2019). The Brg1 ChIP-seq and publicly available datasets reads were mapped to the mouse genome (GRCm38 – mm10) using bowtie2 (v2.3.3.1) (Langmead and Salzberg, 2012). Reads were sorted using samtools (v1.9) (Li et al., 2009); duplicates were removed by picard tools (v2.9.2). Coverage bigwig files were created using bamCoverage from deeptools (v3.3.1) (Ramírez et al., 2016). Peak calling was performed with MACS2 (v2.1.2) using input samples as control (Zhang et al., 2008). For progenitor cell Brg1 ChIP-seq and pro-B cell EBF1 ChIP-seq peak calling peaks with -log10 (q value) threshold of > 10 were selected.

Heatmaps were created using plotHeatmap function from the deeptools (v3.3.1) package (Ramírez et al., 2016). The overlap between different ChIP-seq peaks and genomic features was performed using ChIPpeakAnno (v3.16.0) package from Bioconductor (Zhu et al., 2010) and bedtools2 (v2.27.0) (Quinlan, 2014). Motif enrichment analysis was performed using CentriMo (v4.11.1) (Bailey and Machanick, 2012). ChIP-seq tracks were visualized using the IGV genome browser (Thorvaldsdóttir et al., 2013). Brg1 ChIP-seq bigwig files and read counts were normalized for ChIP efficiency (from EBF1-independent peaks) calculated as: number of reads in EBF1-independent peaks/total number of reads. EBF1-independent peaks were obtained by overlap of all Brg1 ChIP-seq datasets and EBF1wt ChIP-seq dataset.